TOBB UNIVERSITY OF ECONOMICS AND TECHNOLOGY
INSTITUTE OF NATURAL AND APPLIED SCIENCES

OSCILLATORY FLOW FORCED CONVECTION IN A SHALLOW ENCLOSURE WITH SINUSOIDAL BOTTOM WALL TEMPERATURE

M. Sc. THESIS

Saeid RAHEIMPOUR ANGENEH

Department of Mechanical Engineering

Supervisor: Assoc. Prof. Dr. Murat Kadri AKTAŞ

April 2017

Approval of the Graduate School of Science and Technology.

…………………………..

Prof. Dr. Osman EROĞUL
Director

I certify that this thesis satisfies all the requirements as a thesis for the degree of Master of Science.

…………………………..

Assoc. Prof. Dr. Murat Kadri AKTAŞ
Head of Department

I certify that I have read the thesis named as **"Oscillatory flow forced convection in a shallow enclosure with sinusoidal bottom wall temperature"** prepared by Saeid **RAHEIMPOUR ANGENEH** and presented at 11.04.2017, and that in my opinion it is fully adequate in scope and quality, as a dissertation for the degree of Master of Science.

Supervisor: **Assoc. Prof. Dr. Murat Kadri AKTAŞ**   ....
                         TOBB University of Economics and Technology

Examining Committee members:

              Prof. Dr. Şenol BAŞKAYA (Chair)   ....
              Gazi University

              Prof. Dr. Ünver KAYNAK   ....
              TOBB University of Economics and Technology

TEZ BİLDİRİMİ

Tez içindeki bütün bilgilerin etik davranış ve akademik kurallar çerçevesinde elde edilerek sunulduğunu, alıntı yapılan kaynaklara eksiksiz atıf yapıldığını, referansların tam olarak belirtildiğini ve ayrıca bu tezin TOBB ETÜ Fen Bilimleri Enstitüsü tez yazım kurallarına uygun olarak hazırlandığını bildiririm.

I hereby declare that all the information provided in this thesis has been obtained with rules of ethical and academic conduct and has been written in accordance with thesis format regulations. I also declare that, as required by these rules and conduct, I have fully cited and referenced all material and results that are not original to this work.

Saeid RAHEIMPOUR ANGENEH

ABSTRACT

Master of Science

OSCILLATORY FLOW FORCED CONVECTION IN A SHALLOW ENCLOSURE WITH SINUSOIDAL BOTTOM WALL TEMPERATURE

Saeid RAHEIMPOUR ANGENEH

TOBB University of Economics and Technology
Institute of Natural and Applied Sciences
Mechanical Engineering Science Programme

Supervisor: Assoc. Prof. Dr. Murat Kadri AKTAŞ

Date: April 2017

Effects of acoustic streaming on convective heat transfer in a shallow, air-filled, two-dimensional rectangular enclosure with spatially non-uniform temperature distribution of bottom wall are investigated numerically. Excitation of the sound wave in the enclosure is achieved by a periodic motion of the enclosure left wall. The top wall of the enclosure is isothermal while the vertical walls are adiabatic. Compressible form of the Navier-Stokes equations and energy equation are utilized to simulate the flow and temperature fields in the enclosure and solved by Flux Corrected Transport algorithm. Influences of the vibration amplitude and bottom wall temperature profiles are studied. The results demonstrate that the acoustic streaming pattern depends on the temperature profile of the bottom wall and oscillation amplitude. Structure of the flow field in the enclosure affects the rate of heat transfer. The results obtained may have progressive effect on the design of various heat removal applications.

Keywords: Acoustic streaming, Convective heat transfer, Non-uniform temperature profile.

ÖZET

Yüksek Lisans

SİNÜZOİDAL SICAKLIK DAĞILIMLI ALT DUVARA SAHİP SIĞ KAPALI ALANDA TİTREŞİMLİ AKIŞ YARDIMIYLA ZORLANMIŞ TAŞINIM

Saeid RAHEIMPOUR ANGENEH

TOBB Ekonomi ve Teknoloji Üniversitesi
Fen Bilimleri Enstitüsü
Makine Mühendisliği Anabilim Dalı

Danışman: Doç. Dr. Murat Kadri AKTAŞ
Tarih: Nisan 2017

Alt duvarın mekansal olarak eşit olmayan sıcaklık dağılımına sahip, sığ, hava dolu, iki boyutlu bir dikdörtgen kapalı alan içerisindeki taşınım ısı geçişine akustik akışın etkileri sayısal olarak incelenmiştir. Kapalı alan içerisindeki ses dalgalarının uyarımı, kapalı alanın sol duvarının periyodik hareketi ile sağlanmaktadır. Kapalı alanın üst duvarı izotermal, dikey duvarları ise adyabatiktir. Sıkıştırılabilir Navier-Stokes denklemleri ve enerji denklemi kapalı ortamdaki akış ve sıcaklık alanlarını modellemek için kullanılmıştır ve Akı-Düzeltmeli Taşınım algoritması ile çözülmüştür. Titreşim genliğinin ve alt duvar sıcaklık profillerinin etkileri incelenmiştir. Sonuçlar, ikinci mertebe girdapların, alt duvarın sıcaklık profiline ve titreşim genliğine bağlı olduğunu göstermektedir. Kapalı ortam içerisindeki akış alanının yapısı, ısı aktarım hızını etkiler. Elde edilen sonuçlar, çeşitli ısı geçişi uygulamalarının tasarımı için yardımcı olabilir.

Anahtar Kelimeler: İkinci mertebe girdaplar, Taşınımlı ısı aktarımı, Düzgün olmayan sıcaklık profili.

ACKNOWLEDGEMENT

INDEX

LIST OF FIGURES

LIST OF TABLES

ABBREVIATIONS

PIV   Particle Tracking Velocimetry

LDV   Laser Doppler Velocimetry

FCT   Flux-Corrected Transport

LCPFCT   Laboratory for Computational Physics, Flux-Corrected Transport

LIST OF SYMBOLS

The symbols used in this study are presented below along with their explanations.

Symbols	Explanation
c	Speed of sound
c_p	Specific heat at constant pressure
c_v	Specific heat at constant volume
E	Total energy
Ec	Eckert number
f	Frequency
H	Enclosure height
k	Thermal conductivity
L	Enclosure length
p	Pressure
q	Heat rate
R	Ideal gas constant
Ra	Rayleigh number
Re	Reynolds number
Nu	Nusselt number
t	Time
T	Temperature
u	Axial component of velocity
v	Transverse component of velocity
x	x coordinate
y	y coordinate
λ	Wavelength
μ	Dynamic viscosity
ν	Kinematic viscosity
ρ	Density
ω	Angular frequency

1. INTRODUCTION

Interference of two sinusoidal waves with the same amplitude and wavelength which move in the opposite directions leads to a standing wave [1]. Some points on the standing wave do not oscillate at all. These points are called nodes. Some points have the largest amplitudes and are named as antinodes. These points are the locations on the standing waves at which the fluid has the largest and smallest values of its properties such as pressure and velocity. Figure 1.1 presents the standing waves made with oscillation of a vibrator at different frequencies.
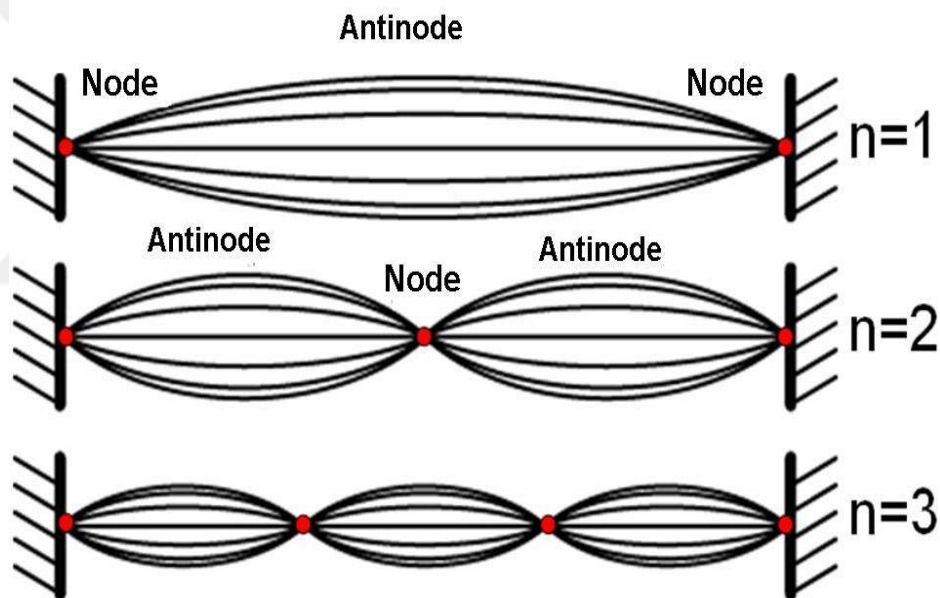
Figure 1.1 : Standing wave patterns at various frequencies of oscillation.

Standing waves are set up at certain values of the oscillation frequencies which are called resonant frequencies. If the vibrator oscillates at a frequency different than a resonant frequency, standing wave is not established. The relation between λ (wavelength), f (resonant frequency), v (speed of travelling wave) and L (fixed distance) is given by:

$$f = \frac{v}{\lambda} = n\frac{v}{2L} \quad for\ n = 1,2,3,\dots \tag{1.1}$$

Mechanical vibrations can produce standing sound waves. Presence of the standing sound waves in a channel filled with viscous fluid induces steady cellular motion of the fluid (acoustic streaming) due to the interaction between the acoustic wave and solid boundaries. These second order, rotational, steady streaming vortices can be classified into three groups as Rayleigh, Schlichting and Eckert streaming.

Schlichting streaming (inner vortices): Inner vortices are formed at the vicinity of the solid boundaries due to the viscous forces and their sizes (in transverse direction) can be determined by the acoustic boundary layer thickness, namely 1.9δ. The acoustic penetration depth is defined as $\delta = (\frac{2\nu}{\omega})^{1/2}$, where ν is the kinematic viscosity and ω is the angular frequency.

Rayleigh streaming (outer vortices): This type of the vortices forms outside the boundary layer and have greater size relative to the inner streaming. The outer vortices have a $\lambda/4$ periodicity and fill the half of the channel approximately.

Eckert streaming: This kind of streaming appears in travelling acoustic wave fields. The formation mechanism of Eckert streaming is completely different than inner and outer streaming.

In this study Rayleigh and Schlichting streaming are considered. Figure 1.2 illustrates the outer and inner streaming rolls.
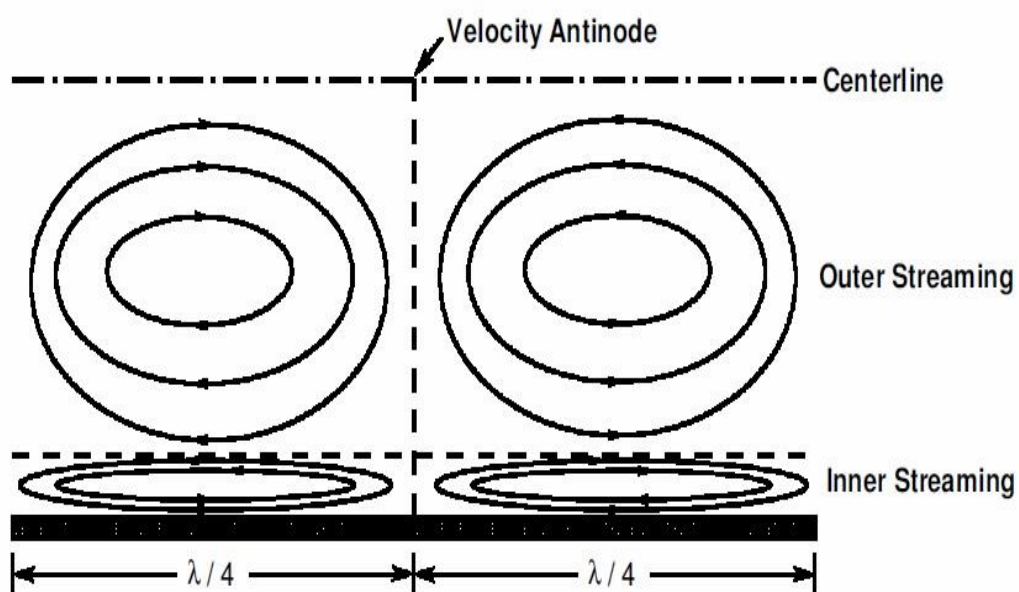
Figure 1.2: Schematic of the inner and outer streaming rolls [2].

Acoustic streaming plays important roles in many applications such as acoustic compressors, thermos-acoustic coolers, ultrasonic surface cleaning and heat exchangers. These second-order vortices affect the heat transfer. Increasing the heat transfer with second order vortices is especially important in areas where the heat transfer with other modes is difficult. For example, acoustic streaming can be used as an aid to heat transfer in such an environment, with low or no gravity since there is no heat transfer by natural convection in these environments. In order to use this technology with all its advantages, it is necessary to understand the nature of acoustic streaming and the associated heat transfer.

1.1. Literature Review

1.1.1. Analytical and numerical investigations

The first theoretical work on acoustic-induced second order vortices was made by Lord Rayleigh [3]. Lord Rayleigh studied the flow of vortices in case of a longitudinal sound field in a Kundt tube. Rayleigh worked on outer vortices and the results found were independent of the viscosity of the fluid. Schlichting [4] considered an incompressible oscillating flow over a flat plate and investigated the patterns of the streaming inside the boundary layer. A general vorticity equation was obtained by Westervelt [5], and a method to evaluate the streaming velocities generated by standing sound wave was developed.

Andres and Ingard [6, 7] studied acoustic streaming formed around a cylinder for both low and high Reynolds numbers ($Re = \frac{U_0 R}{\nu}$ where U_0 stands for the particle velocity, R is the cylinder radius and ν represents the kinematic viscosity), analytically. It is revealed that the flow structure formed around the cylinder at high Reynolds number has opposite direction compared with the low Reynolds number case.

Kurzweg [8] investigated the heat transfer driven by the sinusoidal oscillatory flow between two reservoirs which maintained at different temperatures and connected to each other by series of circular tubes, analytically. The influence of oscillation amplitude, frequency, Prandtl number and tube diameter on heat transfer is revealed.

Qi worked theoretically on the effect of compressibility on acoustic flow near a solid boundary [9]. It was emphasized that compressibility was a necessary condition for the propagation of acoustic waves, but previous studies were limited to incompressible flow. It is found that compressibility causes high flow velocities outside the boundary layer. Qi and his group [10] investigated the streaming created by acoustic activation in a long wide cylinder, by adding compressibility and heat conduction in their calculations. They analyzed the second order vortices inside the boundary layer. It is found that the x-component of the streaming velocity is a function of compressibility, Prandtl number and specific heat ratio.

Vainstein et al. [11] studied the heat transfer in presence of sound wave between two parallel horizontal flat plates maintained at different temperatures, theoretically. An acoustic Peclet number was defined. In addition, an average Nusselt number based on the Peclet number was derived. Their analysis shows that the existence of a sound field with high frequency and amplitude, affects the heat transfer.

Guo and Sung [12] performed a computational investigation to carry out the effects of oscillating flow on heat transfer in a pipe. Pulsation amplitude of the flow and Womersley number ($\beta = a(^\omega/_\nu)^{1/2}$ where a is the pipe radius, ω indicates the angular frequency and ν is the kinematic viscosity) were used to characterize the flow. Both augmentation and reduction in the heat transfer contingent on the Womersley number are observed for small values of the oscillating amplitude. However heat transfer is always enhanced as a result of high amplitude oscillatory flow.

Effects of oscillatory flow on heat transfer in a pipe in which pipe wall was exposed to constant heat flux were studied analytically by Moschandreou and Zamir [13]. Influences of Prandtl number and oscillation frequency on the heat transfer rate were carried out. It is found that, the rate of heat transfer from wall increases in a certain range of a frequency and reduces out of this range. The rate of heat transfer is augmented with decreasing Prandtl number.

An analytical solution was derived by Hamilton et al. [14] for the streaming which was produced by shaking a two-dimensional rectangular resonator in the x-direction. The essential limitation in this study is that the acoustic wavelength is too larger than oscillatory boundary layer thickness. It is found that the size of the inner vortices

decrease as the wide of the channel is increased. Hamilton et al. [15] extended their work by including the thermal effects in calculations which were also applied for cylindrical tubes. It is reported that the streaming velocities are impressed by a few percent due to the effect of heat conduction and temperature dependent viscosity in both very wide and narrow channels. It is also found that in channels of intermediate widths (10-20 times of the boundary layer thickness) thermal conductivity has a considerable effect on acoustic streaming. The results of the cylindrical tubes analysis are the same with the two dimensional channels.

Kawahashi and Arakawa examined the acoustic streaming in an air-filled rectangular enclosure where the standing sound wave was established by the sinusoidally motion of a piston at one end of the duct [16]. Both the first and second order velocities depend on the amplitude of the oscillation. As the amplitude of vibration increases, deformation in the structure of streaming rolls is observed.

Frampton et al. [17, 18] studied the structure of acoustic streaming in micro-fluidic devices analytically. A cylindrical channel with infinite long rigid walls was considered in which one end was subjected to a longitudinal acoustic wave. It is revealed that with reduction in the channel height, the boundary layer streaming becomes dominant while the mean flow velocity remains unchanged. The obtained results show that the acoustic streaming may be effective in micro-fluid control applications.

Aktas and Farouk [19] numerically examined the formation of the second-order vortices produced by acoustic vibration in a rectangular enclosure filled with compressible gas. The sound field in the resonator was induced by the harmonic motion of the enclosure left wall. In this research, effects of the vibrating wall displacement and the enclosure height on the vortex structures were investigated. To obtain Rayleigh streaming structure (streaming rolls have a λ /4 periodicity), the maximum displacement of the oscillating wall must be reduced as the enclosure height increases. Reduction in the left wall displacement amplitude cannot form the regular Rayleigh streaming in the wide resonators (H/L=0.14 where H and L indicate the enclosure height and length). The greater height and wall displacement increase the number of streaming cells.

Carlsson et al. [20] studied the streaming pattern in an incompressible fluid, enclose between two infinite long parallel plates which vibrate in transverse direction, theoretically. They examined the streaming structure in terms of two parameters: frequency and channel height. Four different types of streaming flows depend on these parameters are formed in the channel.

Heat transfer from a rigid wall subjected to sinusoidal temperature profile with an oscillatory flow was studied by Ramos et al. [21]. They assumed incompressible flow with uniform axial velocity. It is found that the heat transfer from the wall remains zero for different values of oscillating velocity amplitudes.

A numerical investigation was carried out to study the effect of acoustic streaming on convective heat transfer in an air filled rectangular enclosure in which the horizontal walls were kept at different temperatures by Aktas and Ozgumus [22]. The results demonstrate that the transverse temperature gradients have significant influence on streaming patterns. The streaming structure formed in the resonator affects the heat transfer.

Daru et al. [23] performed a numerical investigation to study the transition behavior of the acoustic streaming from regular to irregular streaming. They considered a two-dimensional rectangular enclosure filled with air and shaken in the longitudinal direction. It is found that, the presence of the high intensity waves causes to distortion of the streaming rolls and the core of the streaming vortices shifts towards the velocity nodes.

Influence of enclosure shape on the accumulation of acoustic streaming was studied numerically by Cervenka and Bednarik [24]. Excitation of the acoustic field in the resonant cavities was achieved by the shaking of the entire body in the longitudinal direction. They considered resonators with three different shapes as rectangular, wedged and elliptical. It is revealed that the structure of the streaming pattern depends strongly on the shape of the resonators.

1.1.2. Experimental investigations

Ro and Loh [25] experimentally examined the influence of the acoustic streaming on convective heat transfer in a gap spaced between a beam and a heated source. The parameters affecting the heat transfer are reported as the vibration amplitude, the gap

size and the temperature of the cooled object. With increase of the vibration amplitude and temperature difference between the heated source and working fluid (air), heat transfer is augmented.

Oscillatory air flow created by harmonic and sinusoidal motion of a piston in a closed vertical resonance tube was examined numerically and experimentally by Alexeev et al. [26]. They discussed the effects of adiabatic boundary condition on the flow structure. Temperature of air increases due to the heat generation by shock waves in the tube. As a result, the speed of sound is enhanced and causes to achieve a frequency other than resonance frequency which leads a non-periodic oscillatory flow. However, the results obtained from experimental investigations show that the flow is almost periodic and contradict this theory. With considering isothermal boundary condition, heat interactions induce reduction in pressure amplitude alter the oscillation phase and cause a periodic flow.

Jun et al. [27] investigated the contribution of the oscillatory flow to heat transfer in a pipe, experimentally. They discussed the influence of hydrodynamic parameters and the shape of the resonator on heat transfer. The results demonstrate that the increment in the flow rate and the length of the resonator, increase the heat transfer gradually.

An experimental investigation by using the Laser Doppler Velocimetry (LDA) method was performed to carry out the acoustic streaming formed by a standing acoustic wave in an air-filled cylindrical resonator tube by Thompson et al. [28]. It is found that at comparatively low acoustic amplitudes, the variation of the x-component of the outer second-order velocity along the resonator length is sinusoidal, has parabolic shape along the tube height, and is the quadratic function of the acoustic amplitude. Thompson et al. [29] explored the effects of axial temperature gradient produced thermoacoustically and fluid inertia on the outer streaming with the same experimental technique. As the induced temperature gradient increases, streaming velocity decreases, and considerable deformation in the structure of the streaming roll is observed.

Convective heat transfer induced by acoustic streaming between two horizontal plates studied experimentally and numerically by Hyun et al. [30]. Formation of

acoustic streaming in the gap was accomplished by the vibration of the lower beam in the transverse direction while the heated upper beam was kept stationary. They discussed the streaming structure and its effects on the heat transfer. The greater gap size causes reduction in the maximum streaming velocity. However, increment in the vibration amplitude leads to increase in streaming velocity. It is also reported that the considerable temperature drop is achieved in presence of streaming.

Wan et al. [31] studied the influence of the acoustic streaming on convective heat transfer in a narrow channel filled with air, computationally and experimentally. Streaming flow field in the channel was established by vibration of the bimorph in y-direction. The upper beam was stationary with heat source attached. Particle Tracking Velocimetry (PIV) method was used in the experimental procedure. It is revealed that the induced acoustic streaming augments the heat transfer from the heated source to the air. Both the numerical and experimental results demonstrate that the acoustic streaming plays an important role in cooling process.

Moreau et al. [32] performed an experiment to analyze the inner and outer streaming cells, generated in an air-filled cylindrical tube via loudspeakers at the two ends of the resonator. Measurements of the streaming velocities were achieved by using Laser Doppler Velocimetry (LDV) method. In order to characterize the streaming, the Reynolds number ($Re = (\frac{U}{c})^2 (\frac{R}{\delta})^2$ where U is the acoustic velocity amplitude, R is the radius of the tube, c denotes the speed of sound, and δ is the acoustic penetration depth) with wide range was consumed. Reduction in the normalized axial second order velocity is observed near the middle section of the tube with increasing of the Reynolds number. It is also reported that at the Reynolds number approximately equal to 70 two additional streaming vortices appear at the vicinity of the enclosure wall.

An experimental investigation performed by Nabavi et al. [33] to study of the regular and irregular acoustic streaming in an air-filled rectangular enclosure by using Particle Tracking Velocimetry (PIV) technique. They used streaming Reynolds number ($Re = 1/2(\frac{u_{max}}{c})^2 (\frac{H}{\delta})^2$ where u_{max} and c denote the maximum acoustic velocity in the enclosure and the speed of sound, H is the resonator height and δ is the acoustic penetration depth) to classify the regular and irregular streaming. It is revealed that when the steaming Reynolds number is greater than 50, the regular

streaming patterns distort and the complex shapes are formed. In other work, Nabavi and his group [34, 35] studied the effects of horizontally heated walls on streaming structure in an air-filled resonant cavity with PIV method again, experimentally. Presence of the transverse temperature gradient deforms the symmetric shape of the streaming and leads to increment in the streaming velocity.

Reyt et al. [36] performed both experimental and numerical analysis to investigate the formation of acoustic streaming, generated by shaking of an air-filled cylindrical resonator. They used LDV method in the experimental study and considered the compressible form of the Navier-Stokes equations in the numerical analysis. It is found that the cores of the outer streaming rolls are pushed towards the acoustic velocity nodes and new streaming vortices formed in the vicinities of the acoustic velocity antinodes as the Reynolds number ($Re = (\frac{U}{c})^2 (\frac{R}{\delta})^2$) increases.

Tajik et al. [37] studied the influence of acoustic streaming on heat transfer from a heated source located at the top of the water-filled cylindrical enclosure, experimentally. Standing wave in the enclosure was established by the vibration of the bottom plate in the transverse direction with the aid of ultrasonic transducer. The results obtained shows that in presence of acoustic streaming, heat transfer can be improved by about 390%. It is also found that the heat transfer increases as the distance between the heat source and vibrating plate reduces at a given ultrasonic power. Increase in the ultrasonic power also leads to augmentation in heat transfer.

1.1.3. Effects of variable wall temperature on natural convection

Influence of temperature oscillations on natural convection boundary layer near a cylindrical surface studied theoretically by Merkin and Pop [38]. The obtained results show that, in oscillations with high frequency and large times, a steady flow is formed outside the boundary layer.

A numerical investigation of free convection in an enclosure with spatially sinusoidal temperature distribution of heated wall was carried out by Saeid [39]. It is found that length of heat source and amplitude of the sinusoidal temperature profile affect the heat transfer in the cavity. Augmentation in average Nusselt number is observed as the heat source length or temperature profile amplitude increases.

Bilgen et al. [40] investigated the laminar natural convection in an enclosure of which one side wall was exposed to sinusoidal temperature profile, numerically. It is found that, thermal penetration strongly depends on the Rayleigh number and enclosure aspect ratio.

Varol et al. [41] studied the natural convection in a rectangular enclosure in which, bottom wall subjected to spatially sinusoidal temperature profile, numerically. It is revealed that increase in the aspect ratio of the enclosure causes reduction in heat transfer. As the amplitude of temperature profile increases, heat transfer is enhanced.

Wang et al. [42] studied the transient natural convection between two infinite horizontal walls with sinusoidally oscillating temperature profiles, numerically. Time-averaged heat flux from the lower to the upper wall is observed even though the time-average temperature difference between walls is zero. The same result was obtained for different values of temperature oscillation frequency, Grashof number and the distance between walls.

1.2. Research Needs

None of the investigations in the literature considered the influence of non-uniform temperature profiles on the acoustic streaming and associated heat transfer. Thus this study mainly focuses on the influence of the non-uniform temperature profile on the streaming pattern and corresponding heat transfer. To the best of authors' knowledge, this is the first examination of the influence of nonzero mean vibrational flow on the thermal convection from a surface with non-uniform temperature distribution. The results obtained may have useful effect on the design of various heat removal applications.

2. PROBLEM DESCRIPTION AND MATHEMATICAL MODEL

A two-dimensional rectangular resonator filled with air is considered. In order to produce standing wave, the left wall of the enclosure vibrates in the longitudinal direction with lowest resonant frequency. Both horizontal and side walls are rigid. The schematic view of the problem is presented in Figure 2.1.
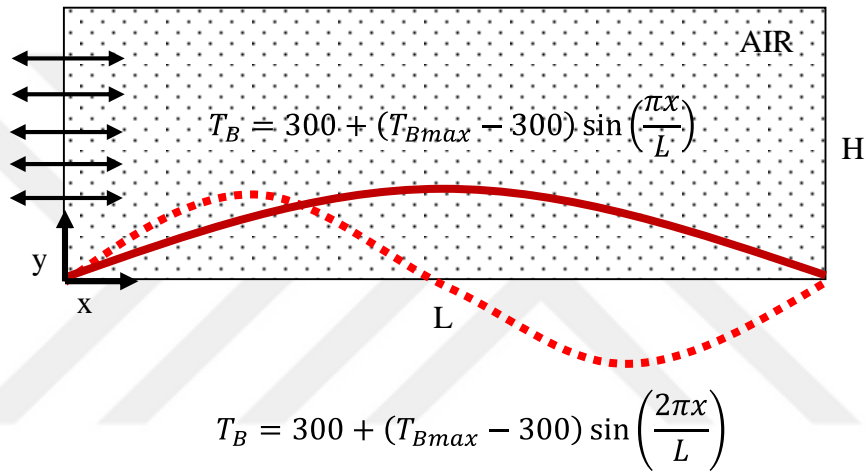
Figure 2.1: Schematic view of the problem.

The harmonic displacement and velocity of the vibrating wall are given by:

$$x(t) = x_{max} \sin(\omega t) \tag{2.1}$$

$$u(t) = \omega x_{max} \cos(\omega t) \tag{2.2}$$

Here, x_{max} symbolizes the maximum displacement amplitude of the left wall and ω represents the angular frequency, $\omega = 2\pi f$. The oscillation frequency is set as $f = 1\ kHz$ and related to the wavelength of the sound wave by $\lambda = c_0/f$, where c_0 is the reference speed of sound in air ($c_0 = 347\ m/s$). The enclosure length is half of the wavelength of sound wave, $L = \frac{\lambda}{2} = 173.5$ mm and the height of the enclosure is $H = 40\delta$. Here, δ is the thickness of the acoustic boundary layer and given by

$\delta = \sqrt{\frac{2\nu}{\omega}}$ .The thickness of acoustic boundary layer is approximately 0.07 mm in this study.

The side walls of the enclosure are adiabatic. The top wall is isothermal and kept at 300 K. The bottom wall of the enclosure is exposed to sinusoidal and half-sinusoidal temperature profiles.

2.1. Governing Equations

The compressible form of the continuity, momentum and energy equations are considered to simulate the flow and temperature fields in the enclosure. In two dimensional Cartesian coordinates, these equations are given as:

$$\frac{\partial \rho}{\partial t} + \frac{\partial (\rho u)}{\partial x} + \frac{\partial (\rho v)}{\partial y} = 0 \tag{2.3}$$

$$\rho \frac{\partial u}{\partial t} + \rho u \frac{\partial u}{\partial x} + \rho v \frac{\partial u}{\partial y} = -\frac{\partial p}{\partial x} + \frac{\partial \tau_{xx}}{\partial x} + \frac{\partial \tau_{xy}}{\partial y} \tag{2.4}$$

$$\rho \frac{\partial v}{\partial t} + \rho u \frac{\partial v}{\partial x} + \rho v \frac{\partial v}{\partial y} = -\frac{\partial p}{\partial y} + \frac{\partial \tau_{yy}}{\partial y} + \frac{\partial \tau_{xy}}{\partial x} \tag{2.5}$$

$$\frac{\partial E}{\partial t} + \frac{\partial}{\partial x}[(E+p)u] + \frac{\partial}{\partial y}[(E+p)v]$$

$$= \frac{\partial}{\partial x}[u\tau_{xx} + v\tau_{xy}] + \frac{\partial}{\partial y}[u\tau_{xy} + v\tau_{yy}] \tag{2.6}$$

$$- \frac{\partial q_x}{\partial x} - \frac{\partial q_y}{\partial y}$$

In equations above, t represents the time, x and y refer to the Cartesian coordinates, u and v indicate the velocity components, p is pressure and ρ is density. The components of the shear stress, heat flux and total energy are expressed as:

$$\tau_{xx} = \frac{4}{3}\mu \frac{\partial u}{\partial x} - \frac{2}{3}\mu \frac{\partial v}{\partial y} \tag{2.7}$$

$$\tau_{yy} = \frac{4}{3}\mu \frac{\partial v}{\partial y} - \frac{2}{3}\mu \frac{\partial u}{\partial x} \tag{2.8}$$

$$\tau_{xy} = \mu \left(\frac{\partial u}{\partial y} + \frac{\partial v}{\partial x} \right) \tag{2.9}$$

$$q_x = -k \frac{\partial T}{\partial x} \tag{2.10}$$

$$q_y = -k \frac{\partial T}{\partial y} \tag{2.11}$$

$$E = \frac{p}{\gamma - 1} + \frac{1}{2}\rho(u^2 + v^2) \tag{2.12}$$

Here, γ is the ratio of specific heats (c_p/c_v) and T is temperature. The change of dynamic viscosity (μ) and thermal conductivity (k) with temperature is followed by the polynomial equations below:

$$\mu(T) = -8.73 \times 10^{-7} + 8.99 \times 10^{-8}T - 1.09 \times 10^{-10}T^2 + 8.3 \times 10^{-14}T^3 \tag{2.13}$$

$$k(T) = -1.97 \times 10^{-3} + 1.2 \times 10^{-4}T - 1.09 \times 10^{-7}T^2 + 6.79 \times 10^{-11}T^3 \tag{2.14}$$

Figure 2.2 compares the viscosity and thermal conductivity values computed with equations above and tabulated values in Incropera [43]. The results are in good agreement.
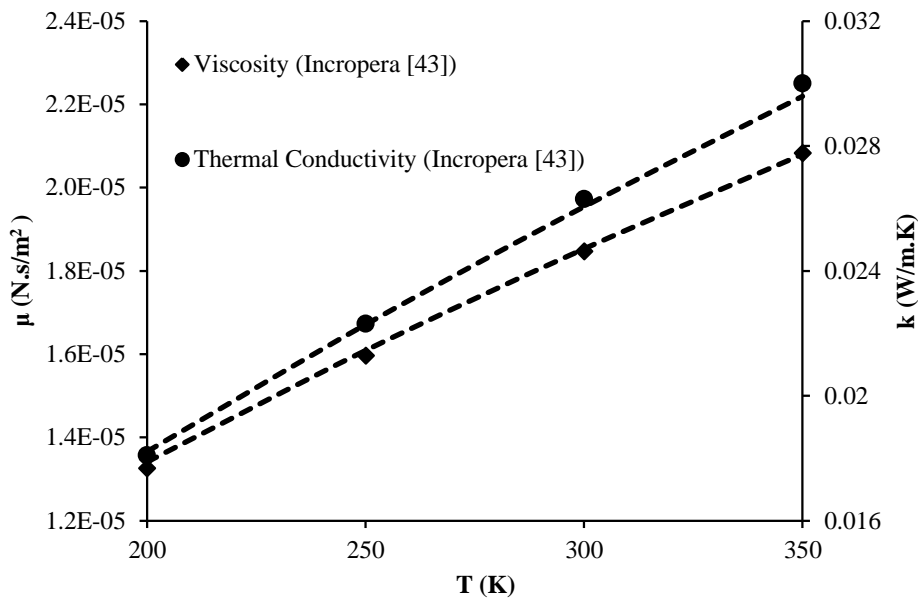

Figure 2.2: Viscosity and thermal conductivity of air as a function of temperature.

The pressure, density and temperature are related to each other by the ideal gas law:

$$p = \rho RT \tag{2.15}$$

here R denotes the specific gas constant.

2.2. Computational Technique

In order to solve the convective part of the equations, an explicit, finite-volume based, Flux-Corrected Transport algorithm is utilized. The diffusion terms are discretized by the central-difference method and added to the solution as a source term. Numerical dispersion and dissipation terms which appear in the numerical scheme result in amplitude and phase errors in the solution. For example in calculations where density is being evaluated, negative density values become visible as a result of oscillations. In order to eliminate or reduce these errors numerical damping terms are added to the calculation process. Consider a numerical scheme in which a damping term is added in a predictor step and a certain amount of damping is removed in a corrector step [44]. Such a numerical scheme is called Flux-Corrected Transport which was developed by Boris and Book [45]. The Flux Corrected Transport (FCT) algorithm is a high-order, non-linear, monotone, conservative, and positivity preserving algorithm developed to solve time-dependent, one-dimensional, nonlinear general continuity equation. This algorithm has fourth order phase accuracy and can solve sharp gradients with minimum numerical diffusion [46].

Consider one-dimensional continuity equation with a three point explicit finite difference formula. Temporary value of density is obtained from the values of previous time step as below:

$$\frac{\partial \rho}{\partial t} + \frac{\partial (\rho u)}{\partial x} = 0 \qquad (2.16)$$

$$\begin{aligned}
\tilde{\rho}_i = \rho_i^0 &- \frac{1}{2}\left[\varepsilon_{i+\frac{1}{2}}\,(\rho_{i+1}^0 + \rho_i^0) - \varepsilon_{i-\frac{1}{2}}\,(\rho_i^0 + \rho_{i-1}^0)\right] \\
&+ \left[\nu_{i+\frac{1}{2}}\,(\rho_{i+1}^0 - \rho_i^0) - \nu_{i-\frac{1}{2}}\,(\rho_i^0 - \rho_{i-1}^0)\right] \\
&= \rho_i^0 - \frac{1}{\Delta x}\left[f_{i-\frac{1}{2}} - f_{i+\frac{1}{2}}\right]
\end{aligned} \qquad (2.17)$$

where $f_{i\pm\frac{1}{2}}$ indicate inflow and outflow fluxes of density across the cell boundaries.

$\varepsilon_{i\pm\frac{1}{2}}$ are convective fluxes which are given as:

$$\varepsilon_{i+\frac{1}{2}} = u_{i+\frac{1}{2}}\,\frac{\Delta t}{\Delta x} \qquad (2.18)$$

14

$$\varepsilon_{i-\frac{1}{2}} = u_{i-\frac{1}{2}} \frac{\Delta t}{\Delta x} \qquad (2.19)$$

$v_{i \pm \frac{1}{2}}$ are non-dimensional numerical diffusion coefficients.

An anti-diffusion stage of FCT algorithm is defined as:

$$\rho_i^n = \tilde{\rho}_i - f_{i+\frac{1}{2}}^{ad} + f_{i-\frac{1}{2}}^{ad} \qquad (2.20)$$

where $f_{i \pm \frac{1}{2}}^{ad}$ are anti-diffusive fluxes and are given as:

$$f_{i-\frac{1}{2}}^{ad} = \mu_{i-\frac{1}{2}} (\tilde{\rho}_i - \tilde{\rho}_{i-1}) \qquad (2.21)$$

$$f_{i+\frac{1}{2}}^{ad} = \mu_{i+\frac{1}{2}} (\tilde{\rho}_{i+1} - \tilde{\rho}_i) \qquad (2.22)$$

here $\mu_{i \pm \frac{1}{2}}$ are anti-diffusion coefficients.

Addition of these anti-diffusion fluxes may cause the appearance of a new maximum or minimum in calculation process. In order to prevent these maxima and minima which appear in the anti-diffusive stage, anti-diffusion fluxes are replaced by corrected fluxes as:

$$\rho_i^n = \tilde{\rho}_i - f_{i+\frac{1}{2}}^{c} + f_{i-\frac{1}{2}}^{c} \qquad (2.23)$$

The corrected fluxes satisfy:

$$f_{i+\frac{1}{2}}^{c} = S \cdot max \left\{ 0, min \left[S \cdot (\tilde{\rho}_{i+2} - \tilde{\rho}_{i+1}), \left| f_{i+\frac{1}{2}}^{ad} \right|, S \cdot (\tilde{\rho}_i - \tilde{\rho}_{i-1}) \right] \right\} \qquad (2.24)$$

$|S|=1$ and its sign is same with the sign of $(\tilde{\rho}_{i+1} - \tilde{\rho}_i)$. If sign of $(\tilde{\rho}_{i+1} - \tilde{\rho}_i)$ is positive, then corrected flux gives:

$$f_{i+\frac{1}{2}}^{c} = min \left[(\tilde{\rho}_{i+2} - \tilde{\rho}_{i+1}), \mu_{i+\frac{1}{2}}(\tilde{\rho}_{i+1} - \tilde{\rho}_i), (\tilde{\rho}_i - \tilde{\rho}_{i-1}) \right] \qquad (2.25)$$

or

$$f_{i+\frac{1}{2}}^{c} = 0 \qquad (2.26)$$

whichever is larger. The anti-diffusion flux is inclined to decrease ρ_i^n and to increase ρ_{i+1}^n. Thus anti-diffusion fluxes cannot produce a new minimum and maximum during the calculation process.

Calculations were performed with a one-dimensional LCPFCT (Laboratory for Computational Physics, Flux-Corrected Transport) algorithm [47]. In order to apply this algorithm, the two dimensional continuity, momentum and energy equations are divided into two parts resulting in one dimensional equations in x and y directions. After calculation in x direction is done, computation in y direction is performed. A suitable time step must be chosen in order to satisfy the Courant-Friedrichs-Lewy (CFL=$c\Delta t/\Delta x$) criterion.The CFL number is chosen smaller than 0.4 in both x and y directions in this study. Numerical scheme was developed in FORTRAN language for related calculations. Figure 2.4 represents the calculation procedure in flow chart.

In all simulations, typically a 101 x 101 numerical mesh is used which is shown in Figure 2.3. In order to resolve thin oscillatory boundary layer, the grids are generated non-uniformly in transverse direction and clustered at the vicinity of the horizontal walls. The quality of grids gradually decreases towards to middle section. The grid size is uniform along the longitudinal direction. For each period of the pressure waves emanating from the left wall of the enclosure, 100,000 time steps are used.
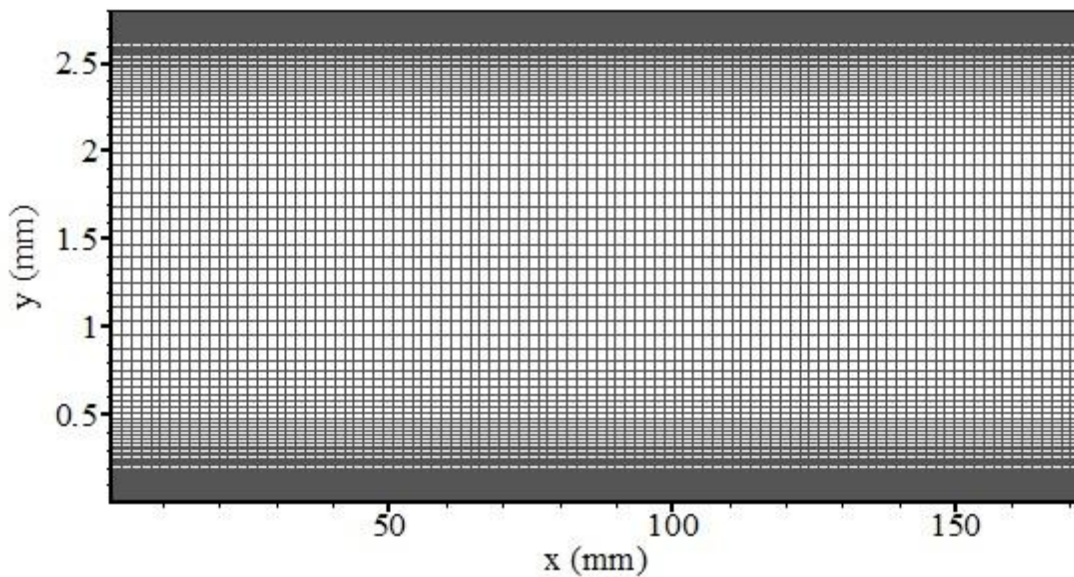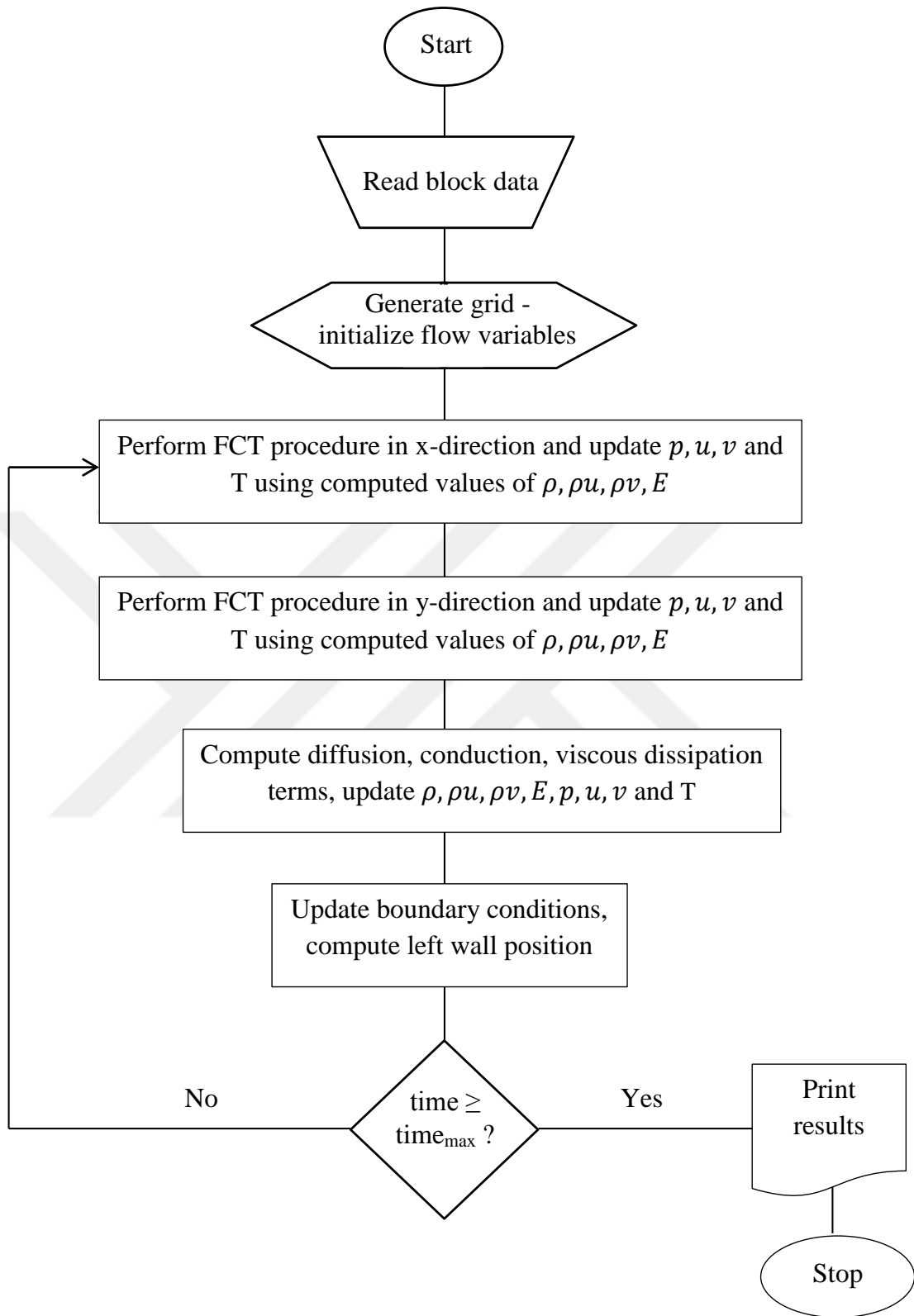

Figure 2.3: 101×101 numerical mesh.

Figure 2.4: Flow chart of FCT scheme [22].

2.3. Initial and Boundary Conditions

The enclosure has no-slip walls. The side walls are adiabatic. A sinusoidal or half-sinusoidal spatial temperature profile is applied to the bottom wall while the top wall is kept at initial temperature. The boundary conditions are:

$$u(0, y, t) = \omega X_{max} \cos(\omega t) \tag{2.27}$$

$$v(0, y, t) = 0 \tag{2.28}$$

$$u(L, y, t) = v(L, y, t) = 0 \tag{2.29}$$

$$u(x, 0, t) = v(x, 0, t) = 0 \tag{2.30}$$

$$u(x, H, t) = v(x, H, t) = 0 \tag{2.31}$$

$$\frac{\partial T}{\partial x}(0, y, t) = \frac{\partial T}{\partial x}(L, y, t) = 0 \tag{2.32}$$

$$T(x, 0, t) = T_B \tag{2.33}$$

$$T(x, H, t) = T_T \tag{2.34}$$

Sinusoidal and half sinusoidal temperature distributions of the bottom wall are expressed as:

$$T_B = 300 + (T_{Bmax} - 300) \sin\left(\frac{2\pi x}{L}\right) \tag{2.35}$$

$$T_B = 300 + (T_{Bmax} - 300) \sin\left(\frac{\pi x}{L}\right) \tag{2.36}$$

In order to obtain the density at boundaries properly, an approach recommended by Poinsot and Lee [48] is used along the stationary no-slip walls as:

$$\frac{\partial \rho}{\partial t}(x, 0) = -\frac{1}{c}\frac{\partial p}{\partial y}(x, 0) - \rho(x, 0)\frac{\partial v}{\partial y}(x, 0) \tag{2.37}$$

$$\frac{\partial \rho}{\partial t}(x, H) = -\frac{1}{c}\frac{\partial p}{\partial y}(x, H) - \rho(x, 0)\frac{\partial v}{\partial y}(x, H) \tag{2.38}$$

$$\frac{\partial \rho}{\partial t}(L, y) = -\frac{1}{c}\frac{\partial p}{\partial x}(L, y) - \rho(L, y)\frac{\partial u}{\partial x}(L, y) \tag{2.39}$$

Since the velocity of the vibrating wall is time-dependent, a modified equation is used to compute the density along the left wall:

$$\frac{\partial \rho}{\partial t}(0, y) = \frac{\gamma \rho(0, y)}{c} \frac{\partial u}{\partial t}(0, y) + \frac{\gamma \rho(0, y)(u(0, y) - c)}{c} \frac{\partial u}{\partial x}(0, y)$$
$$- \frac{\gamma(u(0, y) - c)}{c^2} \frac{\partial p}{\partial x}(0, y)$$

(2.40)

Initial conditions are:

$$p(x, y, 0) = 101325 \, Pa$$ (2.41)

$$\rho(x, y, 0) = 1.1768 \frac{kg}{m^3}$$ (2.42)

$$T(x, y, 0) = 300 \, K$$ (2.43)

The radiation heat exchange between walls in the enclosure is neglected. The particle motion due to free convection occurs in the enclosure when the buoyancy force is large enough, and becomes more important than both viscous forces and thermal diffusion. The critical Rayleigh number for starting motion in the enclosure is about 1708. In this study the maximum value of the Rayleigh number is about 40, and the effect of gravity is neglected also. The Rayleigh number is given by:

$$Ra = \frac{g\beta \Delta T H^3}{\nu \alpha}$$ (2.44)

where g is the gravitational acceleration, β indicates thermal expansion, ΔT represents the temperature difference between the walls, ν is kinematic viscosity and α is thermal diffusivity.

3. RESULTS

3.1. Second-order Vortices Induced by Vibrating Left Wall

In this section effect of the maximum displacement of the left wall on oscillatory and mean flow fields is investigated. The bottom wall of the enclosure is kept at 300 K at this section. Table 3.1 lists the cases simulated.

Table 3.1 : Cases simulated.

Case	x_{max} (μm)	$T_T = T_B$ (K)
A	60	300
B	80	300
C	100	300

Figure 3.1 shows the oscillatory flow field in the enclosure during the 40th acoustic period at various instants for Case A. These instantaneous flow fields remain same at all periods after 40th acoustic cycle, so the flow is named quasi steady-state. It can be noted that instantaneous velocities in the enclosure change spatially and temporally. Left wall of the enclosure moves through the inside of the enclosure and reaches to its maximum displacement value at $\omega t = \pi/2$ where the flow is towards the right wall. The wall moves back to its initial position at $\omega t = \pi$ while flow is still towards the right wall but slows down. At the instant $\omega t = 3\pi/2$, the left wall moves through the out of the enclosure and reaches to its maximum displacement value and extracts the flow towards itself. The left wall then comes back to its initial position at $\omega t = 2\pi$ while the flow is still towards the left wall and slows down. The instant $\omega t = 2\pi$ is identical to the instant $\omega t = 0$ which is the beginning of the next coming cycle. The same pattern can be observed in Case B and C. The maximum values of the x-component of the acoustic velocity in the enclosure reach to 5.5, 7.3 and 9 m/s for Case A, B and C, respectively.
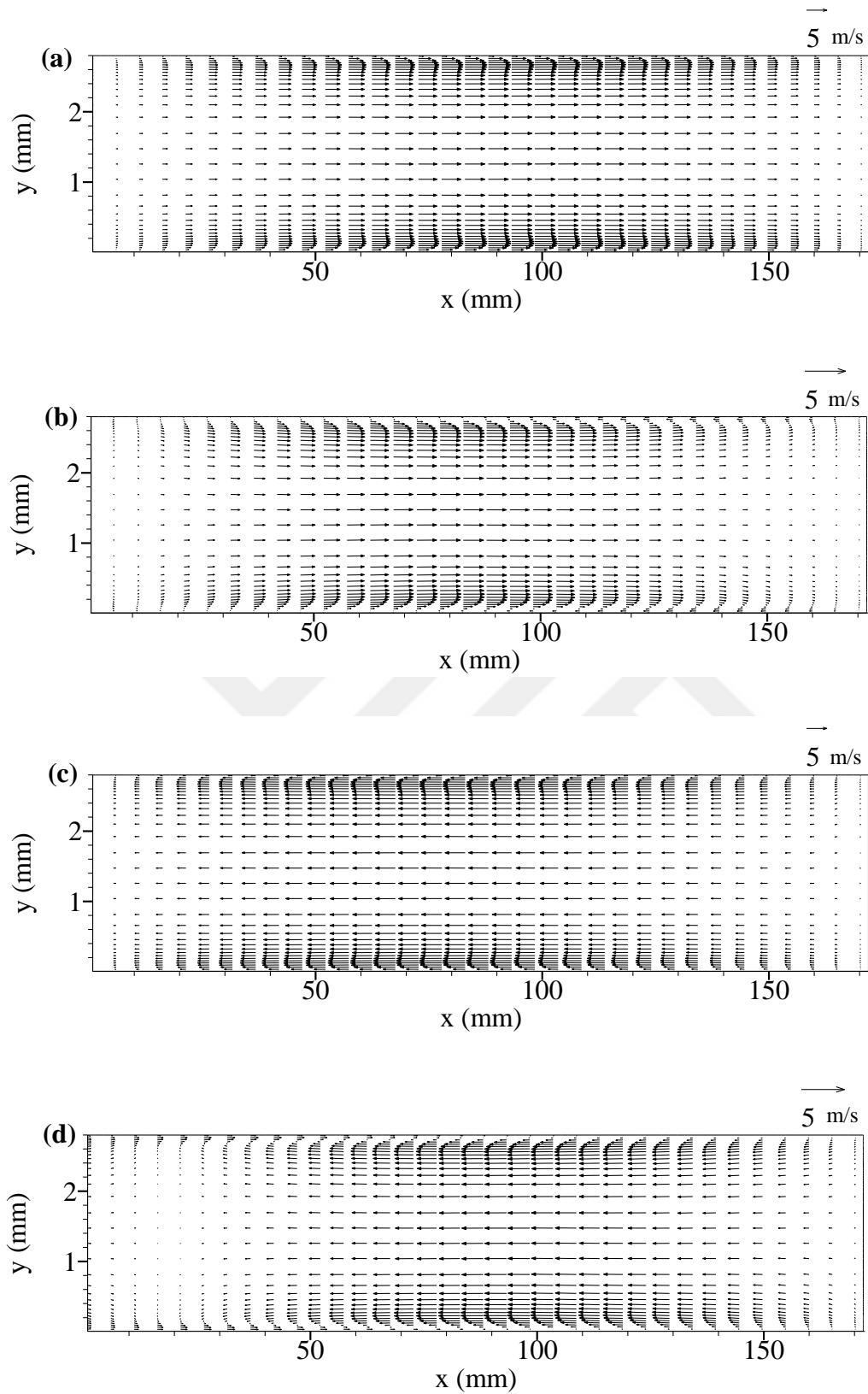
Figure 3.1 : Velocity distributions in the enclosure during 40th acoustic cycle at four instants for Case A: (a) $\omega t=\pi/2$, (b) $\omega t=\pi$, (c) $\omega t=3\pi/2$ and (d) $\omega t=2\pi$.

Figure 3.2 represents the distribution of the pressure and the x-component of the velocity along the horizontal mid plane (y=H/2) of the enclosure at four different instants during the 40th acoustic cycle for Case A. The pressure distributions at four various instants of the acoustic cycle indicate that the pressure node forms near the midpoint of the enclosure length (x≅L/2). The x-component of the velocity at all instants reaches to its maximum value at the same region.

The pressure reaches to its maximum value on the vibrating (left) and minimum value on the stationary (right) wall of the enclosure at ωt=2π and just the opposite behavior can be observed at ωt=π. A closer look on the Figure 3.2.b shows that, x-component of the velocity at both ωt=2π and ωt=π changes its sign at the vicinity of the left wall. The flow is towards the left wall along the enclosure length, up to the vicinity of the vibrating wall where the flow velocity changes its sign and flows towards the right wall due to the motion of the vibrating wall to the right at ωt=2π. At this location where the flows with opposite directions collide, the pressure has its maximum value. At ωt=π, the direction of the flow is towards the right wall in the great portion of the enclosure, while it is towards the left near the oscillating wall which moves to the left. At this point where flows with different directions move away from each other pressure gets its minimum value.

Pressure contours in the enclosure at ωt=π/2, π, 3π/2 and 2π during the 40th cycle for Case A are presented in Figure 3.3. It is obvious that the pressure profiles shown in the Figure 3.2.a remain identical along the any plane from bottom to the top wall in the enclosure.
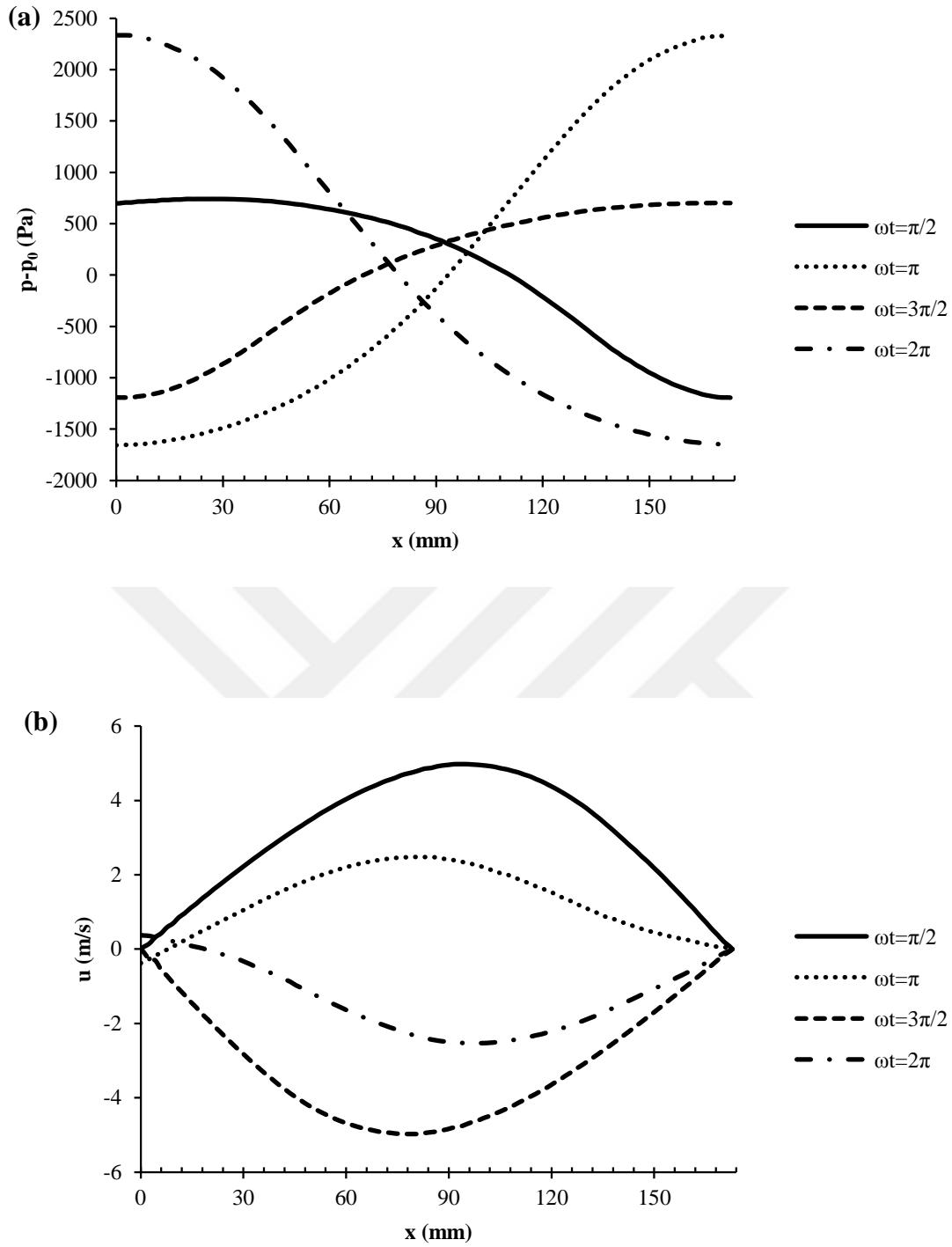
Figure 3.2 : Distribution of (a) pressure and (b) x-component of the velocity along the horizontal mid-plane (y=H/2) of the enclosure during the 40th cycle for Case A at ωt=π/2, ωt=π, ωt=3π/2, and ωt=2π.
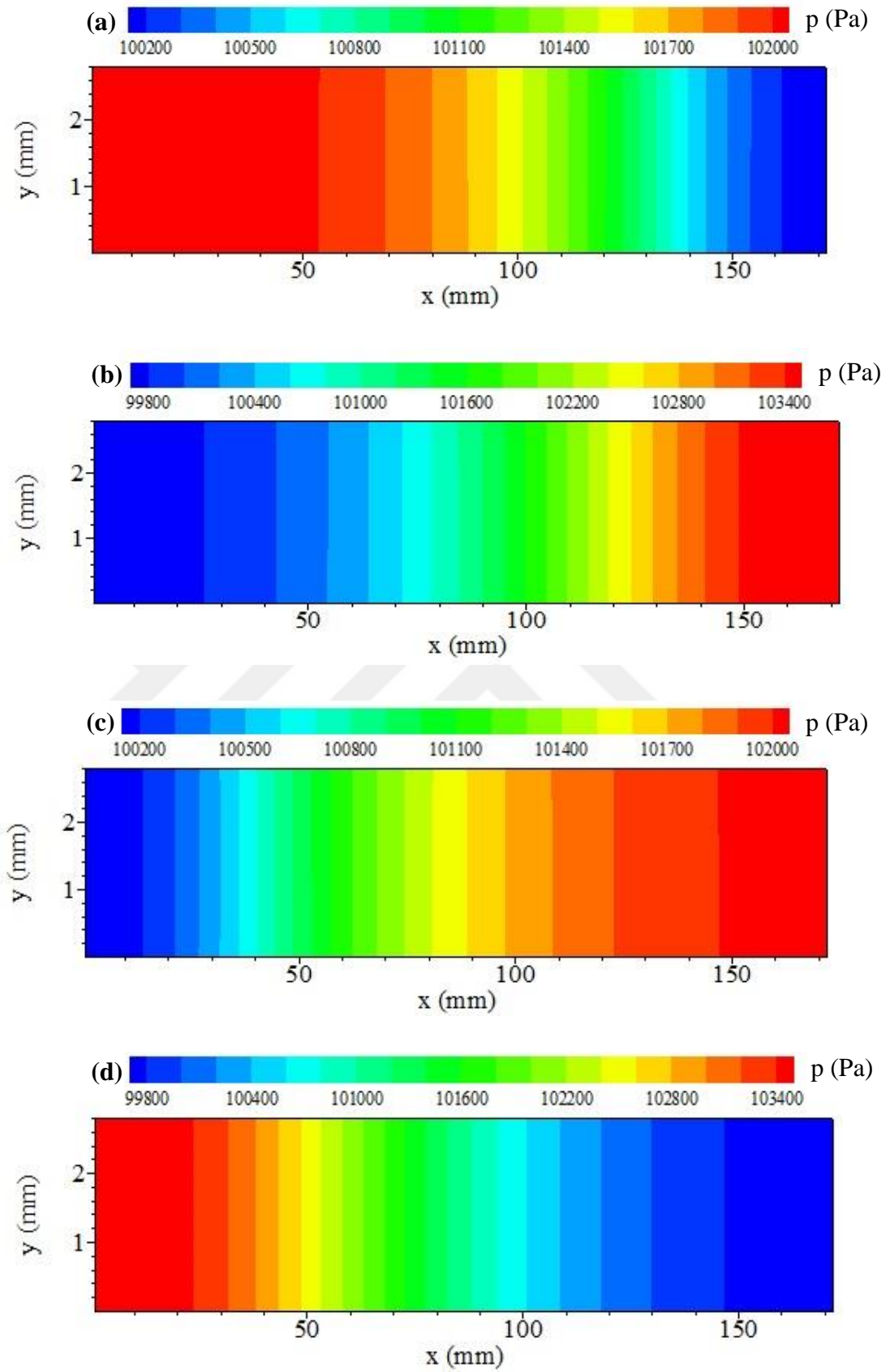
Figure 3.3 : Pressure contours in the enclosure during the 40th cycle for Case A at: (a) ωt=π/2, (b) ωt=π, (c) ωt=3π/2 and (d) ωt=2π.

In order to obtain the steady, secondary flow (acoustic streaming) in the enclosure, the time averaged values of instantaneous density, x- and y-components of the velocity (u and v) are computed during the 40th acoustic cycle and the streaming velocities are obtained at t=0.04 s. By this time, quasi steady values are obtained. Further increase of the number of periods has no effect on the computed velocities. Axial and transverse components of the acoustic streaming velocities are represented as u_{st} and v_{st}, respectively.

$$u_{st} = \frac{\langle \rho u \rangle}{\langle \rho \rangle} \qquad v_{st} = \frac{\langle \rho v \rangle}{\langle \rho \rangle} \qquad (3.1)$$

The symbol $\langle \rangle$ indicates the time average during one vibration cycle of the enclosure left wall. The streaming pattern in the enclosure for Case A at t=0.04 s is shown in the Figure 3.4. Two types of streaming vortices can be observed in Figure 3.4. The first type is the inner streaming formed near the acoustic boundary layer and the second one is the outer streaming extend from the edge of the inner vortices through the middle section of the enclosure. The outer streaming flows towards the velocity nodes and turns back through the velocity antinode along the horizontal mid-plane to accomplish a closed loop. The inner and the outer streaming rolls have opposite direction of rotation. Both inner and outer streaming vortices are fairly symmetric respect to the horizontal and vertical mid-planes.

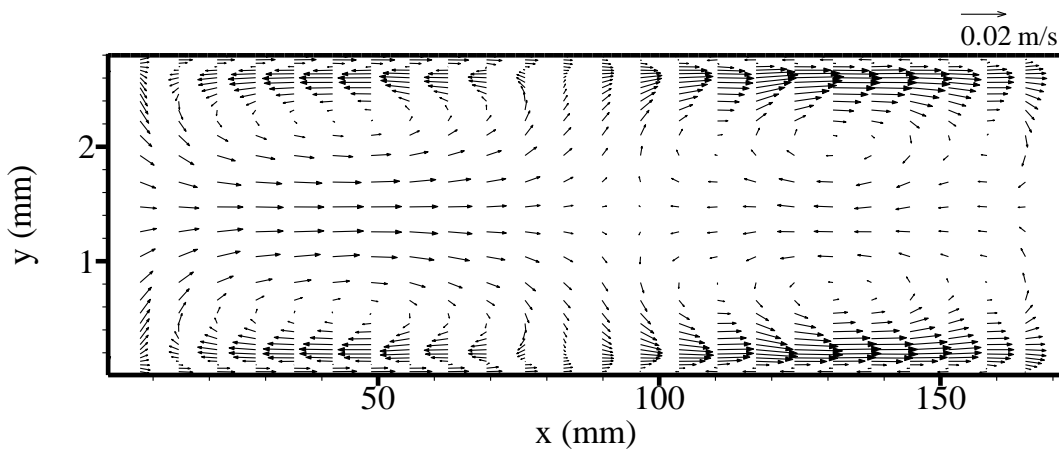
Figure 3.4: Time-averaged flow field in the enclosure at t=0.04 s for Case A.

Figure 3.5 represents the streaming flow field in the enclosure at t=0.04 s for Case B and C. While the symmetry of the streaming cells remains unchanged with increase

in the maximum displacement of the left wall, the remarkable change in the streaming velocities can be observed.
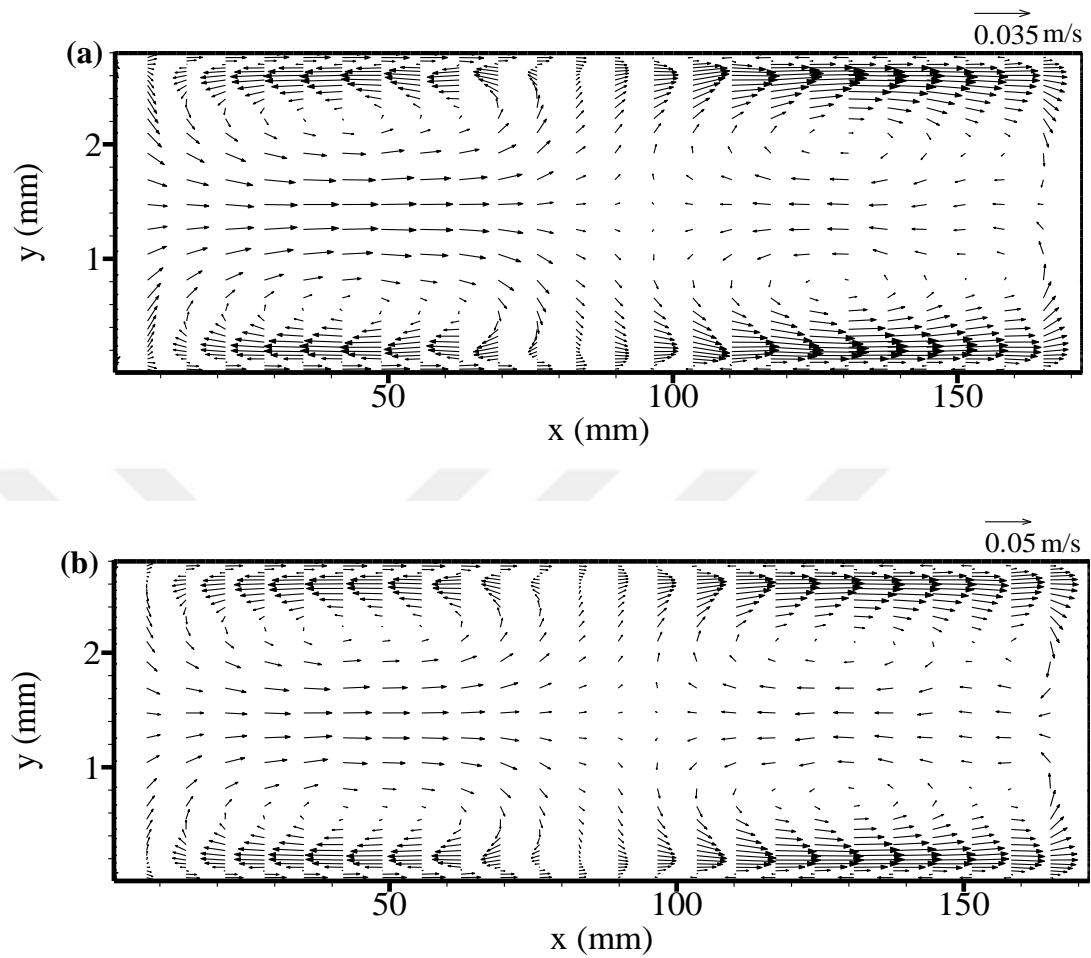

Figure 3.5 : Time-averaged flow field in the enclosure at t=0.04 s for: (a) Case B and (b) Case C.

The simulation results are verified with the analytical solution of Hamilton et al. [14]. The x-component (at x=3L/4) and y-component (at x=L/2) of the streaming velocity along the semi-height (y_0=H/2) of the resonator for Case A are presented in the Figure 3.6. A reference streaming velocity u_R=$3u_{max}^2$/$16c_0$ is used to normalize the velocity values. Here u_{max} is the maximum velocity in the oscillatory flow field. $v_{st}x_0$/$u_R y_0$ is the y-component of the non-dimensional streaming velocity. x_0 denotes the semi length of the enclosure (x_0 = L/2). The results of the current study slightly differ from the reference solution. The velocity profiles shown in the reference study are for a resonator where the excitation of the sound field is achieved by shaking the entire enclosure harmonically. However, the resonator under investigation in this

study is stationary and vibrating a vertical wall produces the sound wave in the enclosure.

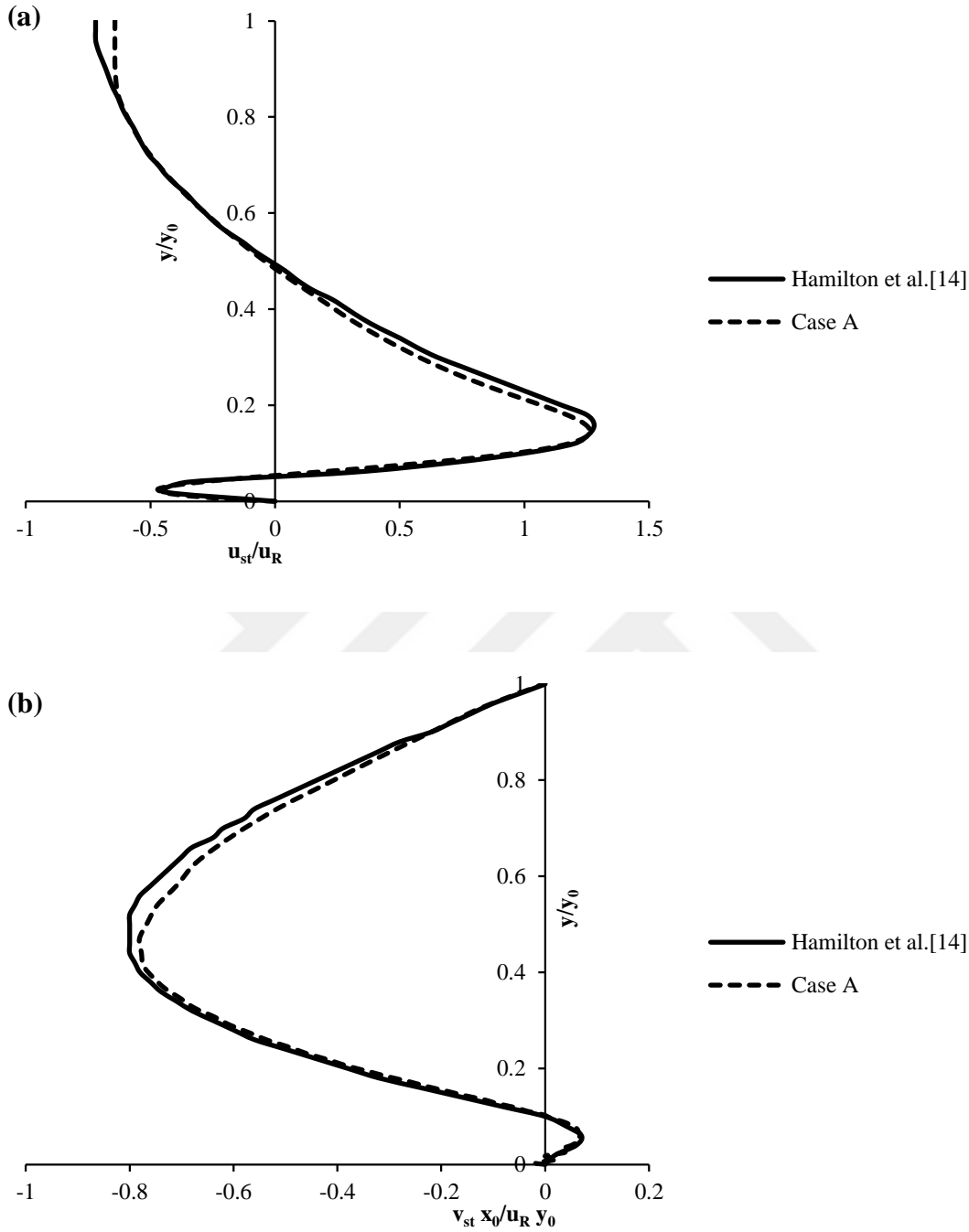Figure 3.6: Non-dimensional streaming velocity profile along the semi height of the enclosure; (a) x-component at x=3L/4 and (b) y-component at x=L/2.

Figure 3.7 illustrates the distribution of the x-component of the acoustic streaming velocity along a vertical line at x=L/4 at t=0.04 s for Case A. In order to show the influence of the grid size on numerical predictions, the results of both coarser

(91×91) and denser (111×111) numerical meshes are added to the figure. The results show that the 101×101 numerical mesh is sufficient to solve the flow pattern.
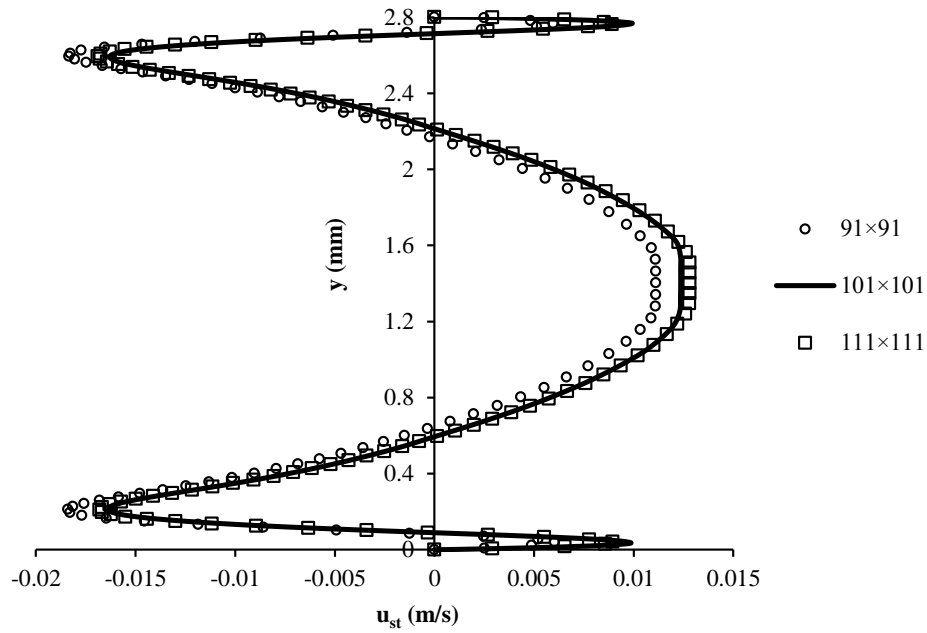

Figure 3.7 : Variation of the x-component of the acoustic streaming velocity along a vertical line at x=L/4 for Case A with different mesh structures.

Variation of the axial component of the second-order velocity along the vertical lines at x=L/4 and x=3L/4 for Case A, B and C are shown in Figure 3.8. Increase in the maximum displacement of the vibrating wall leads to increase in the streaming velocity. In all cases presented here, the symmetric pattern respect to the horizontal mid-plane (y=H/2) can be observed and the classical Rayleigh streaming still exists, although the increment in the maximum displacement of the left wall. Figure 3.9 depicts the distribution of the y-component of the streaming velocity along the enclosure height at x=L/2 for Case A, B and C. The points on the y-axis where the streaming velocity is zero can be considered as the boundary between the streaming rolls. It can be clearly noted that the transverse component of the streaming velocity crosses the y-axis at the same points in all cases.
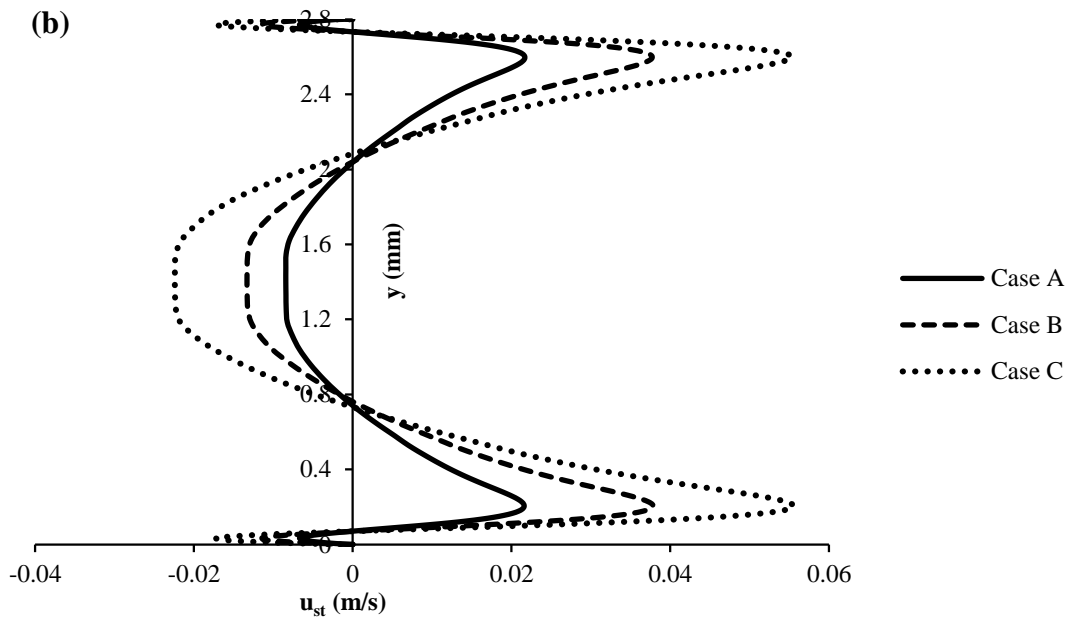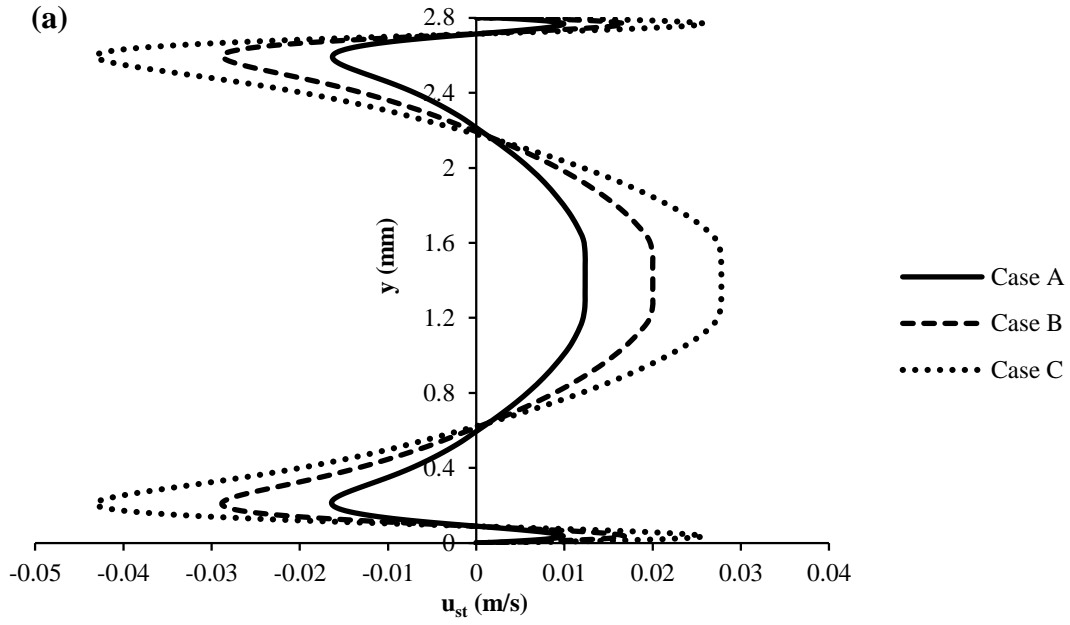
Figure 3.8: Distribution of the x-component of the streaming velocity for Case A, B and C along the vertical lines at (a) x=L/4 and (b) x=3L/4.
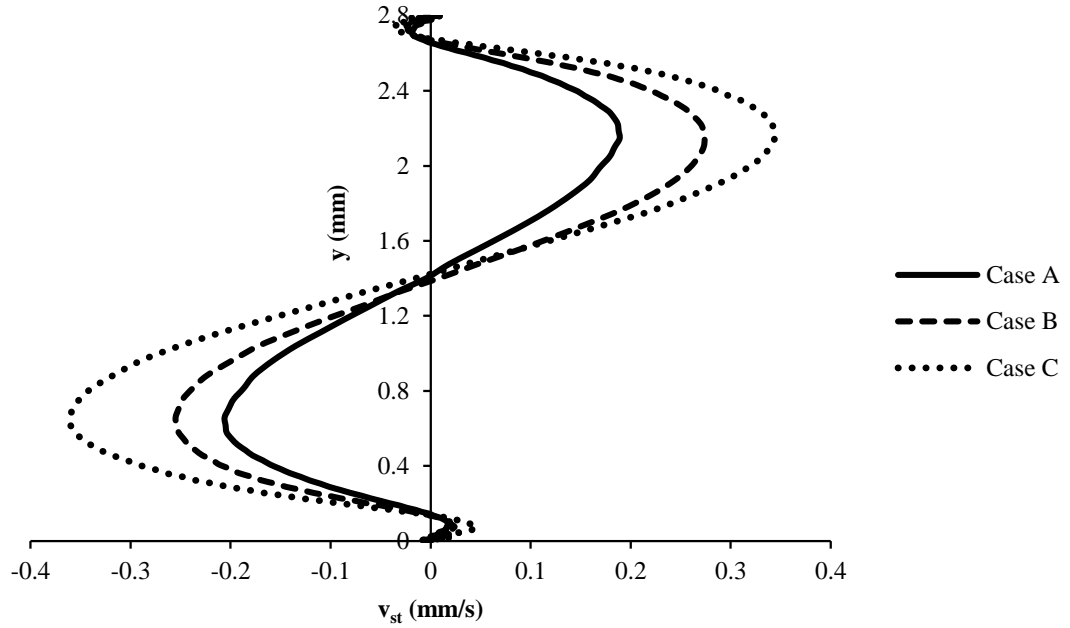
Figure 3.9 : Distribution of the y-component of the streaming velocity for Case A, B and C along the vertical line at x=L/2.

Figure 3.10.a shows the evolution of the pressure with time at the mid-point of the right wall for Case A. The periodic pattern of the primary flow can be observed. Temporal variation of the pressure during the last two periods at the middle of the stationary vertical wall for Case A is presented in Figure 3.10.b. Pressure profile behaves like a sinusoidal wave at each period of sinusoidally harmonic motion of the left wall. A small deviation from the perfect sinusoidal shape can be observed due to the viscous effects.

Variations of the pressure versus time at the mid-point of the right and left walls during the 40th acoustic cycle for Case A, B and C is shown in the Figure 3.11. As the maximum displacement of the vibrating wall increases, the pressure wave with higher amplitude is induced in the enclosure, resulting in an increase in the flow velocity. The pressure amplitudes on both vertical walls are 4380, 5740 and 7030 kPa for Case A, B and C respectively.
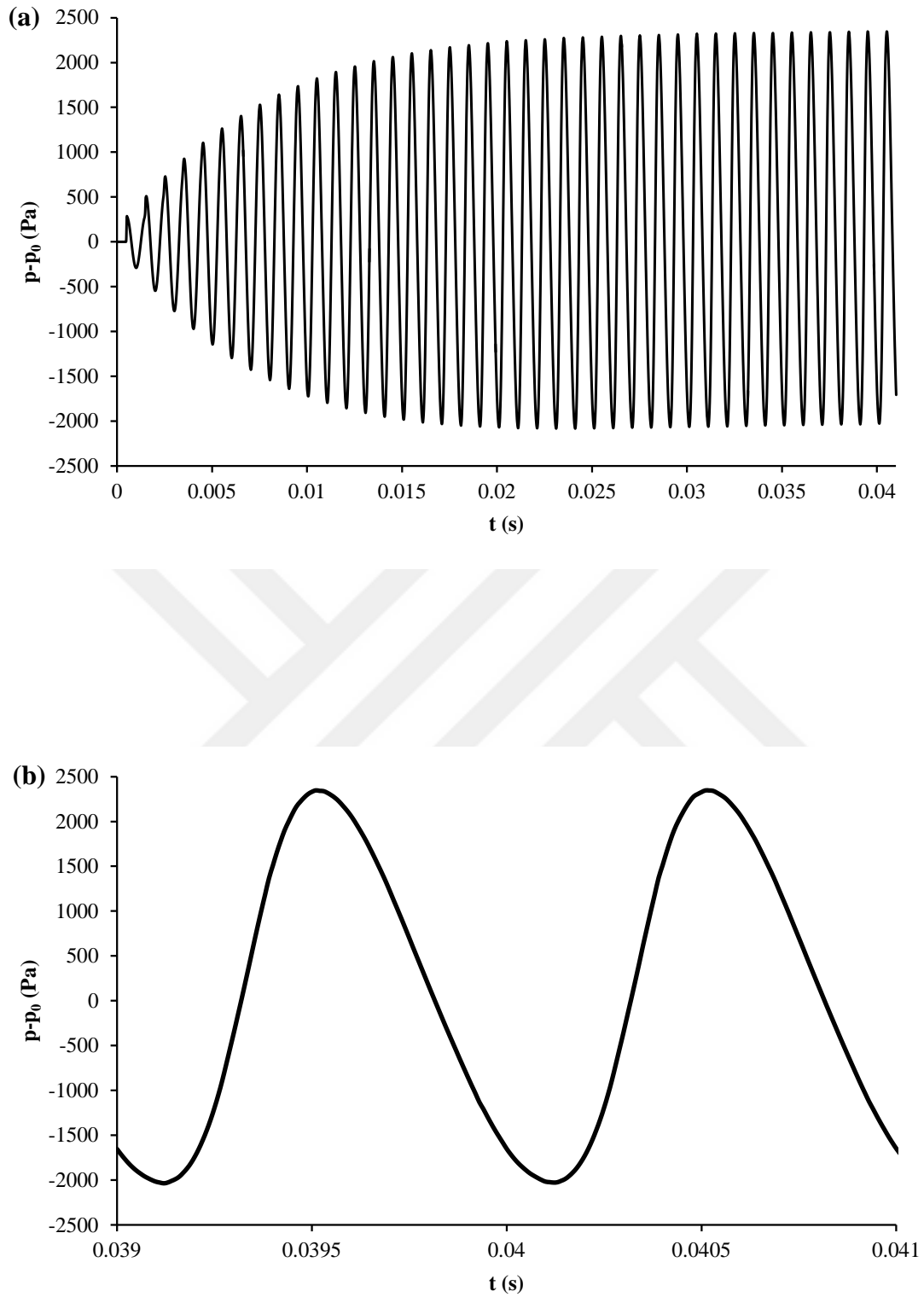
Figure 3.10: Temporal variation of the pressure on the mid-point of the right wall for Case A during (a) all periods and (b) last two periods.

Figure 3.11: Temporal variation of the pressure on the midpoint of (a) left and (b) right walls for Case A, B and C during the 40th acoustic cycle.
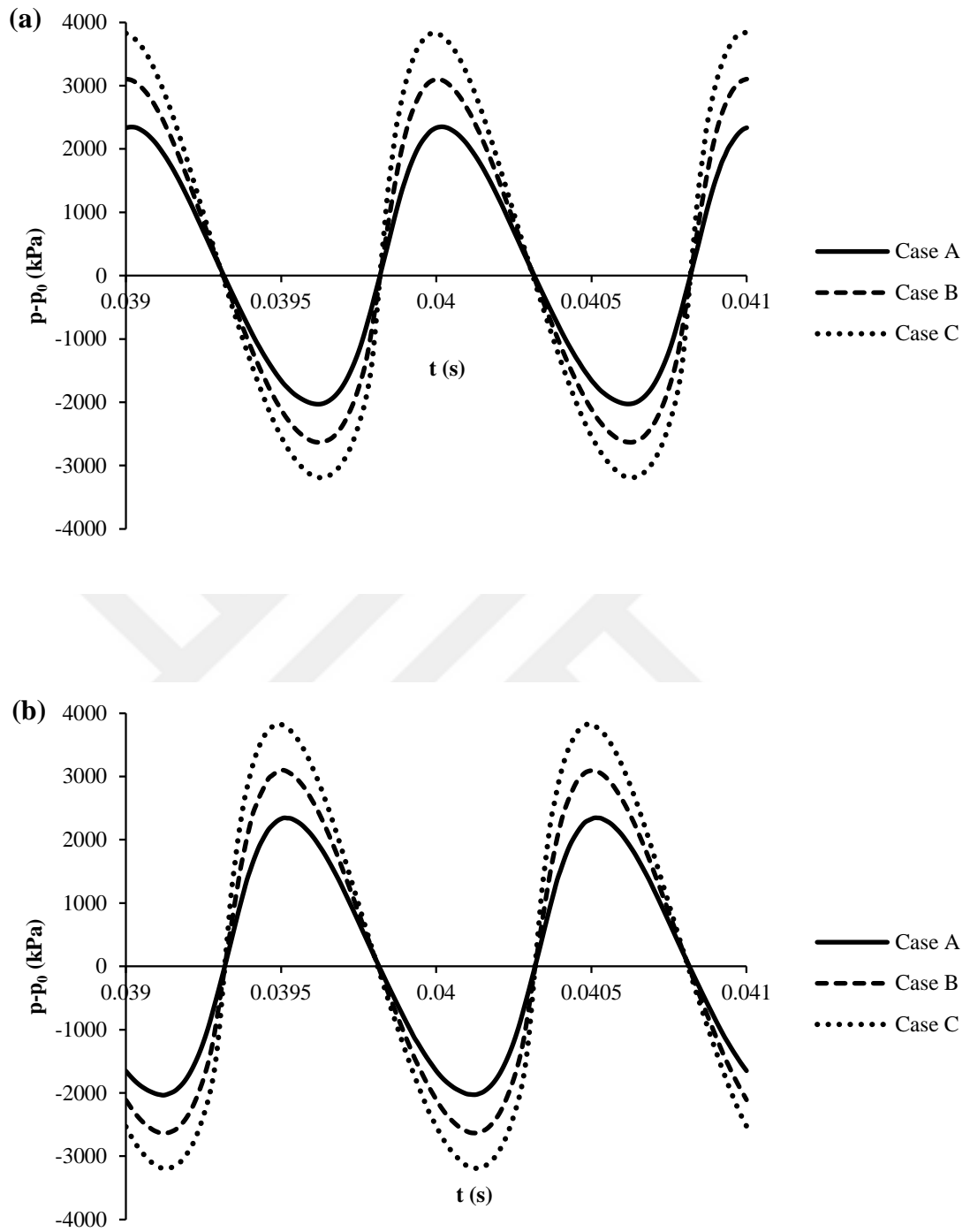
Figure 3.12 shows the variation of the x-component of the velocity with time at the mid-point of the enclosure (x=L/2 and y=H/2) during the last four periods for Case

A, B and C. As the maximum displacement of the left wall is increased velocity is enhanced in the enclosure.
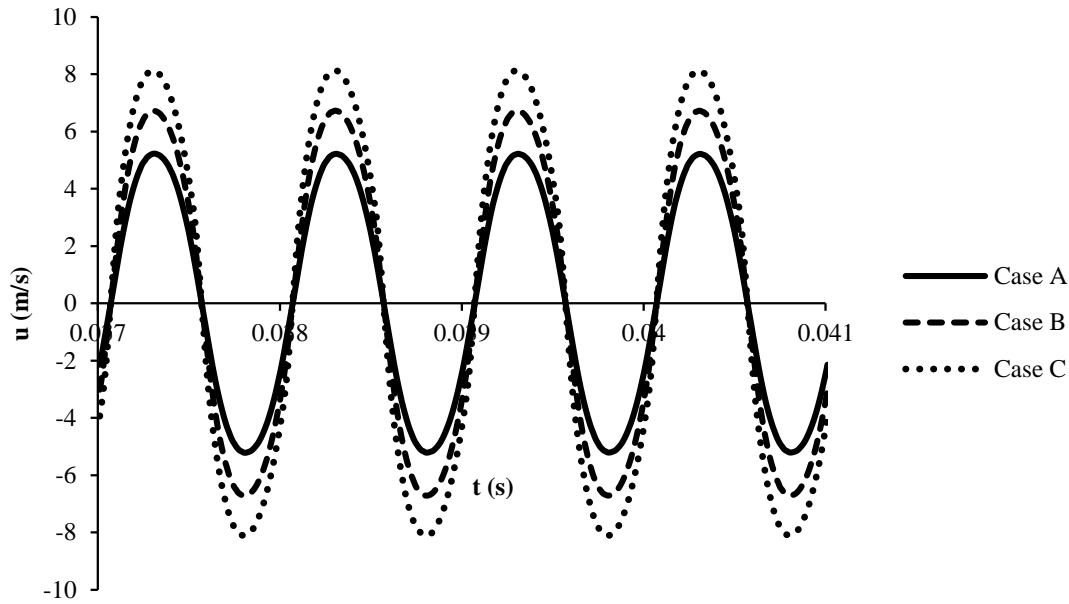
Figure 3.12: Temporal variation of the x-component of the velocity on the midpoint of the enclosure during the last four periods.

3.2. Influence of the Non-uniform Temperature Profile on Streaming Structures and Associated Heat Transfer

This section is devoted to study the effects of the non-uniform temperature profile on the acoustic streaming patterns in the enclosure. The resonator considered in this section has the same dimensions with the enclosure mentioned at the previous section (H=2.8 mm, L=173.5 mm). The formation of the second-order vortices is established by the harmonic motion of the left wall. For each cycle of the harmonic motion of the vibrating wall, 100,000 time steps are used. The side walls of the enclosure are adiabatic and the top wall is isothermal, and kept at 300 K for all cases simulated in this chapter. In order to observe the influence of the non-uniform temperature distribution on the flow structure, two different types of sinusoidal profile are applied as the boundary condition to the bottom wall.

Table 3.2 lists the simulated cases in this section. The maximum displacement of the left wall and the maximum temperature values for the bottom wall having sinusoidal or half-sinusoidal temperature profile are given in the table.

Table 3.2 : Cases considered.

Case	Profile	$T_{Bmax}(K)$	X_{max} (µm)
A-1	sinusoidal	310	
A-2		320	60
A-3	half	310	
A-4	sinusoidal	320	
B-1	sinusoidal	310	
B-2		320	80
B-3	half	310	
B-4	sinusoidal	320	
C-1	sinusoidal	310	
C-2		320	100
C-3	half	310	
C-4	sinusoidal	320	

Figure 3.13 shows the time-averaged flow field in the enclosure for Case A-1 and Case A-3 at the end of the 40th acoustic cycle. The bottom wall of the enclosure is exposed to sinusoidal and half-sinusoidal temperature profiles for Case A-1 and Case A-3, respectively. Presence of the temperature gradients deforms the symmetric structure of the streaming observed in Case A. Expansion in the outer streaming vortices at the vicinity of the bottom wall and contraction in the outer cells near the top wall are observed in Case A-3 as the temperature of the bottom wall increases. Despite the deformation of the Rayleigh streaming structure in Case A-3 due to the temperature rise of the bottom wall, symmetry respect to the central vertical line is still observed. The symmetric nature of the flow is deformed completely in Case A-1. The lower outer streaming roll in the left portion of the resonator expands. Similar pattern is observed for the upper outer vortex in the right portion of the enclosure since the temperature of the top wall is higher in this section. The results demonstrate that the pattern of the flow in the enclosure depends strongly on the applied temperature profile to the bottom wall.
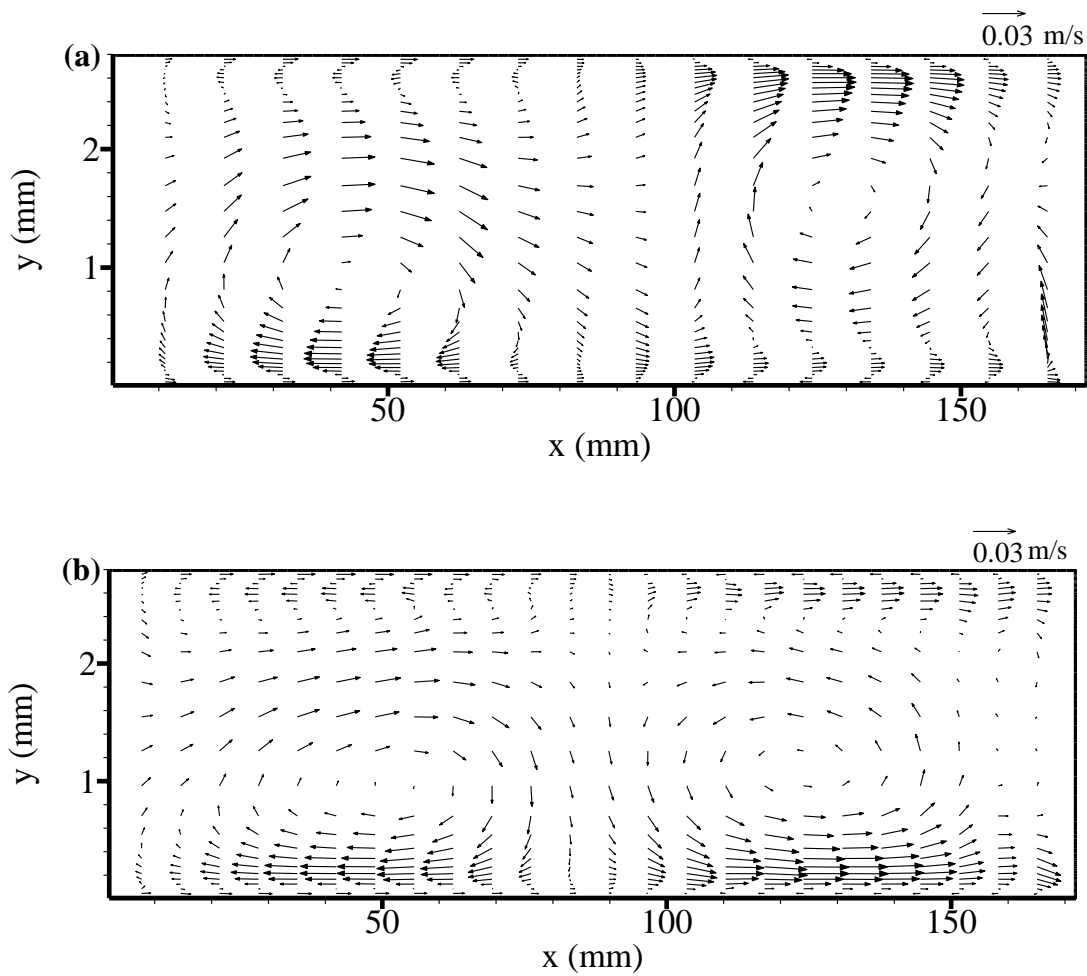
Figure 3.13: Streaming flow field in the enclosure at t=0.04s for (a) Case A-1 and (b) Case A-3.

Figure 3.14 depicts the distribution of the axial streaming velocity along the y-axis through the center of the streaming cells (x=L/4 and x=3L/4) for Case A, A-1 and A-3 at t=0.04s. The axial streaming velocity is perfectly symmetric respect to the horizontal mid-line in both locations in Case A since the temperature of the bottom wall is kept at initial temperature such as top wall. The streaming velocity increases and reaches to its maximum value near the bottom wall in both Case A-1 and A-3 at x=L/4. The maximum positive streaming velocity is observed in Case A-1 since the sinusoidal temperature profile has the maximum wall local temperature at this point (x=L/4). Reduction in the streaming velocity is observed at the vicinity of the bottom wall in Case A-1 at x=3L/4 due to the lowest local temperature of bottom wall at this location.
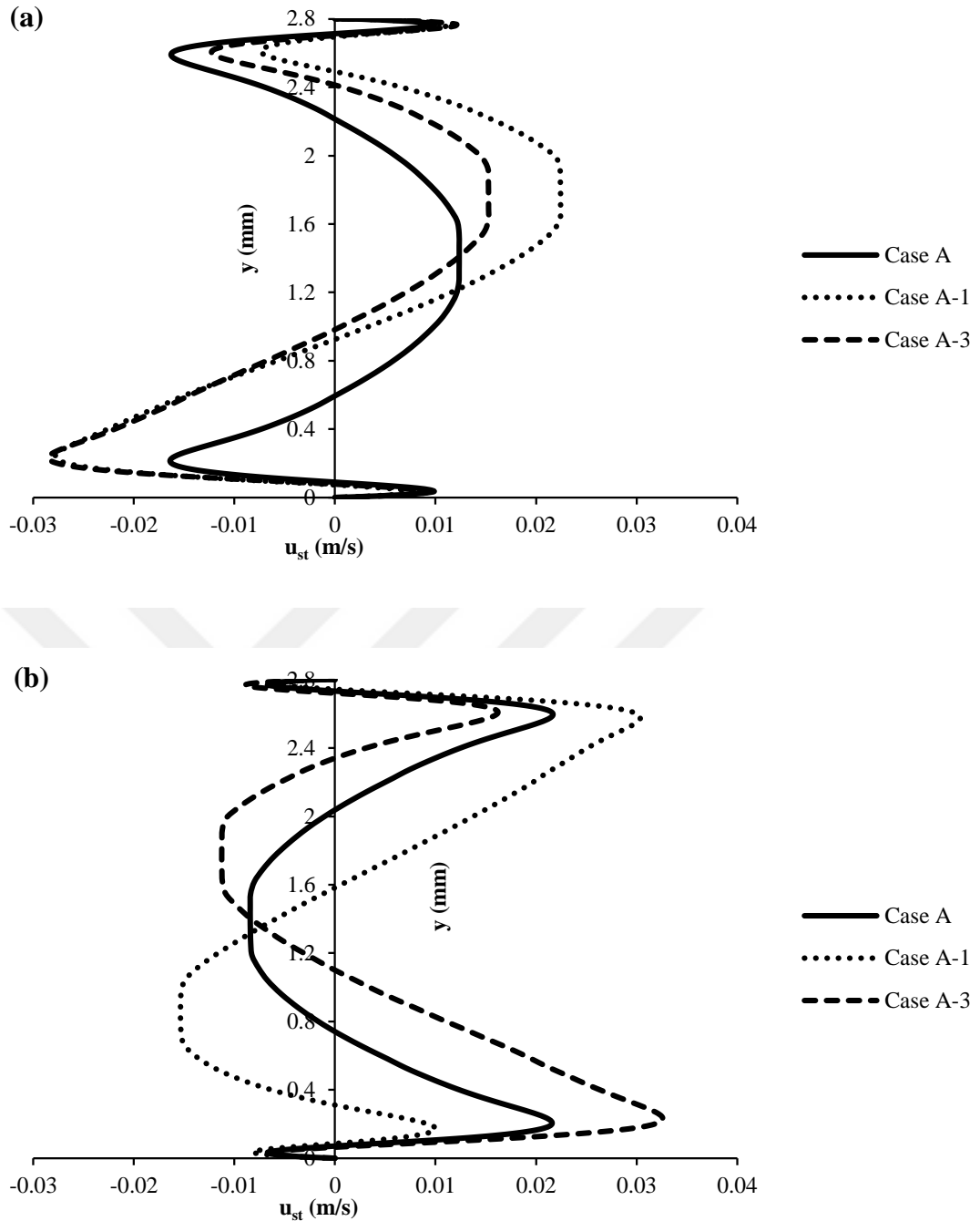
Figure 3.14: Variation of the x-component of the streaming velocity at t=0.04 s along the y-axis at (a) x=L/4 and (b) x=3L/4.

The time-averaged density profile along the vertical lines at x=L/4 and x=3L/4 for Case A, A-1 and A-3 at t=0.04 s is represented in Figure 3.15. Presence of temperature gradients leads to expansion in the streaming vortices, resulting in reduced density (Figure 3.15.a). As the density reduces, the streaming velocity enhances in the rarefied zones which can be observed in Figure 3.14.a in both Case A-1 and A-3. At x=3L/4, air is compressed near the bottom wall due to the low

temperature of the wall at this section in Case A-1. As a result, the streaming velocity reduces in the dense zones. The density profile at both x=L/4 and x=3L/4 remain identical for Case A-3 due to the symmetric pattern of the half-sinusoidal temperature profile.

Figure 3.15: Cycle-averaged density profile along the enclosure height at t=0.04 s for Case A, A-1 and A-3 at (a) x=L/4 and (b) x=3L/4.

Spatially non-uniform bottom wall temperature profiles induce axial and transverse temperature gradients in the enclosure. In order to investigate the transition behavior of the secondary flow due to the gradual enhancement in these gradients, additional cases are considered as listed in Table 3.3.
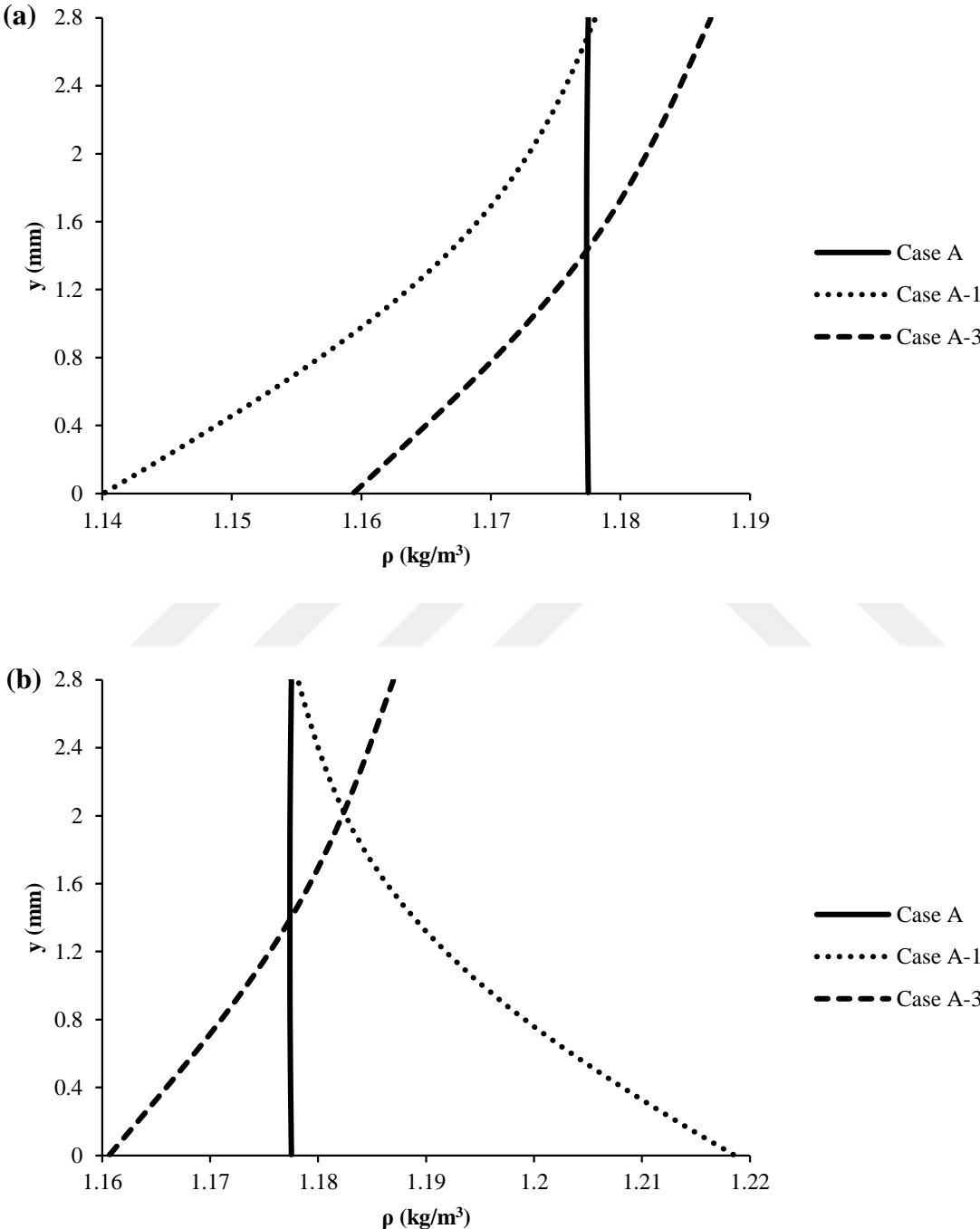
Table 3.3 : Cases with intermediate temperatures.

Case	Profile	T_{Bmax}(K)	X_{max} (µm)
1-a	Half Sinusoidal	300.5	60
1-b		301	
1-c		302	
1-d		304	
1-e		306	
1-f		308	
2-a	sinusoidal	300.5	
2-b		301	
2-c		302	
2-d		304	
2-e		306	
2-f		308	

The maximum displacement of the left wall is set to 60 µm and frequency of the left wall vibration is 1 kHz for all cases listed in Table 3.3. Figure 3.16 and 3.17 depict the cycle averaged flow field in the left portion of the enclosure at t=0.04 s for all cases mentioned here. The streaming velocities increase by the augmentation in the bottom wall temperature. In the half-sinusoidal heating cases (Figure 3.16), as the bottom wall temperature increases, the lower outer streaming vortex expands, and its center shifts towards the top wall and the core of the upper outer streaming roll moves towards the left wall. This is due to the spatial non-symmetry of the bottom wall temperature between $0 < x < L/2$. The outer streaming roll at the bottom section expands in transverse direction and compresses the outer streaming roll at upper section in the sinusoidal heating cases (Figure 3.17). However the core of the upper streaming vortex remains at x=L/4.
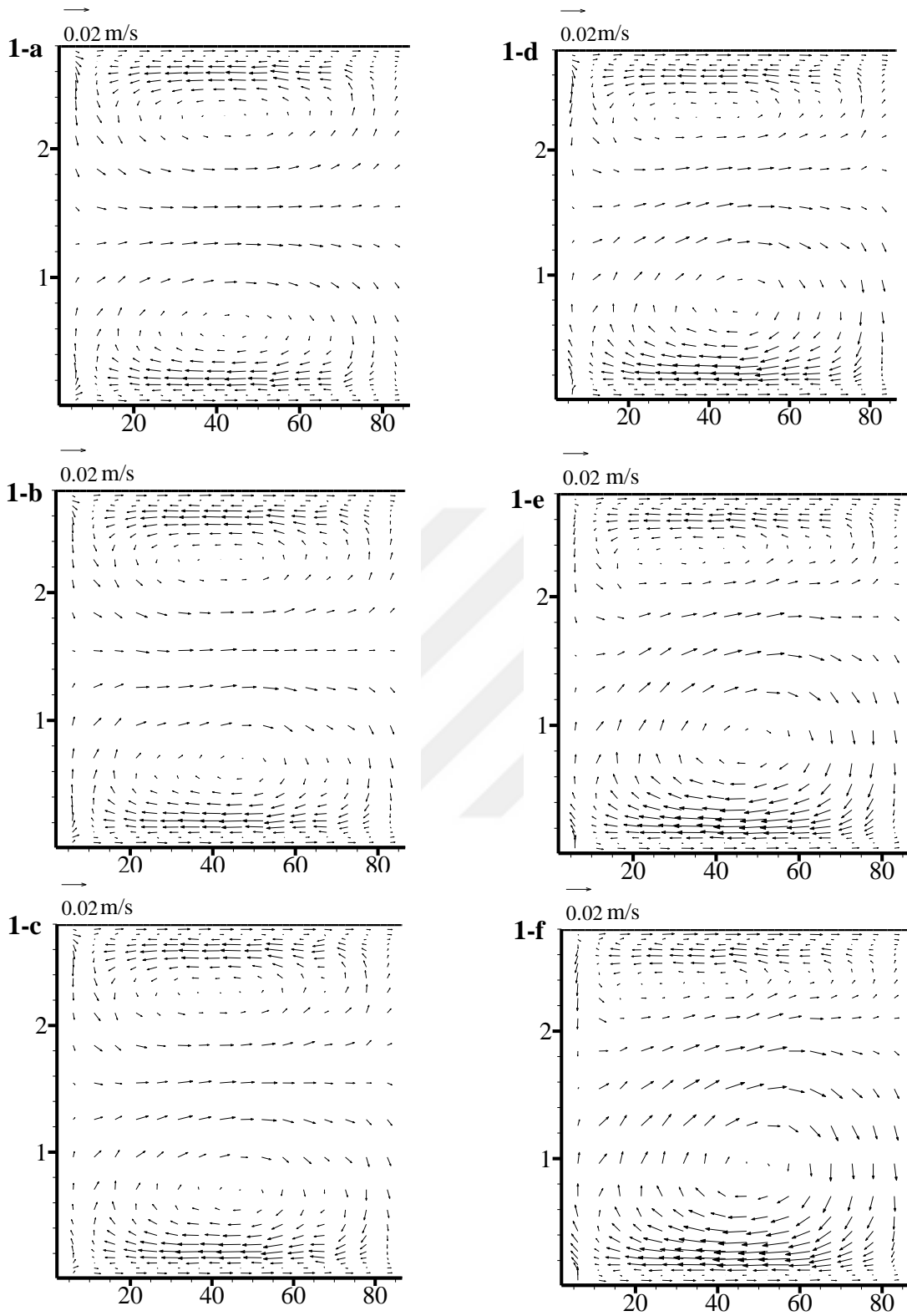
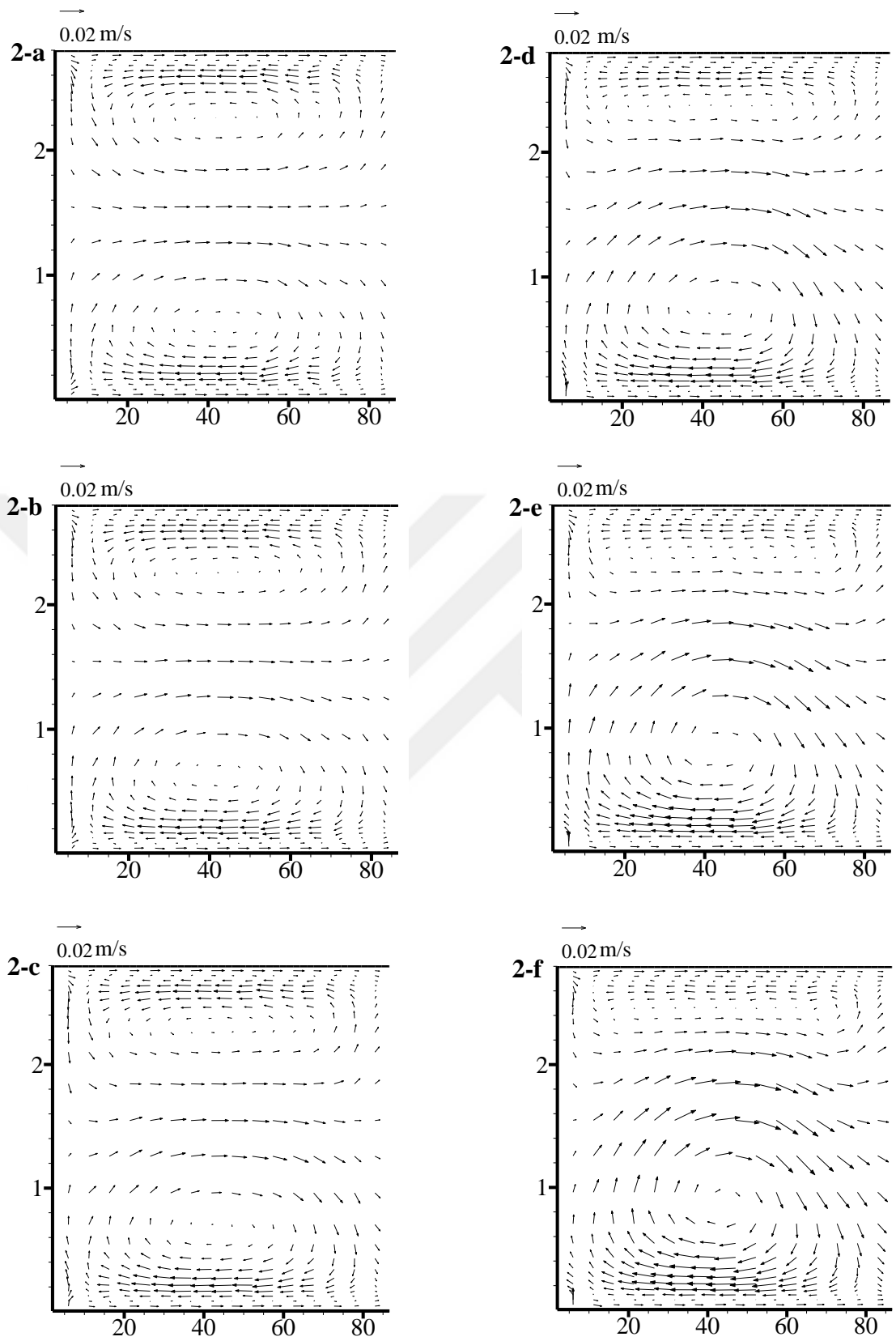Figure 3.16: Streaming flow field for half-sinusoidal cases.

40

Figure 3.17: Streaming flow field for sinusoidal cases.

Figure 3.18 illustrates the time evolution of the pressure on the mid-point of the right wall for all cases with the maximum wall displacement of 60 μm during the last two periods. The pressure amplitude increases due to the increase in the maximum displacement of the left wall as discussed before. An enhancement in the amplitude of the pressure wave is also observed at the fixed maximum wall displacement value when the bottom wall of the enclosure is subjected to the half-sinusoidal temperature profile (Case A-3 and A-4). As the maximum temperature of the half-sinusoidal profile (which is at x=L/2) increases (form 310 to 320 K) the pressure amplitude also increases. The pressure amplitudes are 4610 and 4710 kPa for Case A-3 and A-4 respectively. However, the magnitude of the pressure amplitude remains approximately identical (4380 kPa) in the both sinusoidal cases (Case A-1 and A-2).
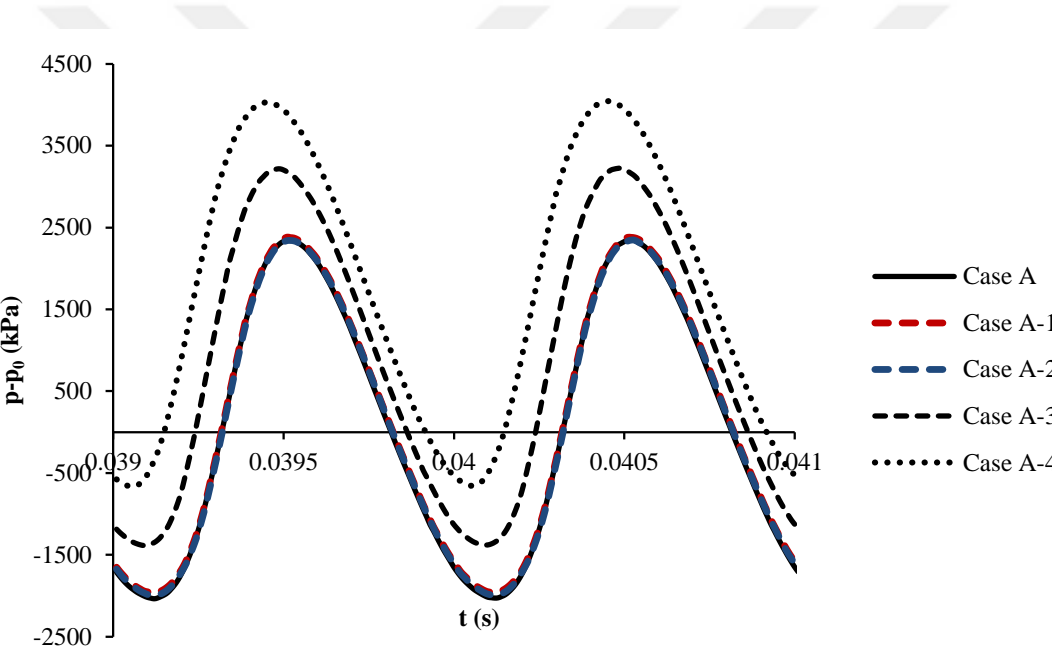
Figure 3.18: Temporal variations of the pressure on the midpoint of the right wall for Case A, A-1, A-2, A-3 and A-4 around the 40th acoustic cycle.

Figure 3.19 indicates the variation of the axial primary velocity with respect to x-axis at y=H/2 for cases with the vibration amplitude of 60 μm at $\omega t=\pi/2$ during the 40th acoustic cycle. Applying half sinusoidal temperature profile to the bottom wall enhances the velocity and augmentation can be observed as the amplitude of the profile increases. However, the same behavior does not occur in the sinusoidal cases, and the velocity remains nearly unchanged. The results obtained demonstrate that,

42

the existence of the temperature difference at the point of the velocity antinode affects the pressure amplitude and the primary velocity.
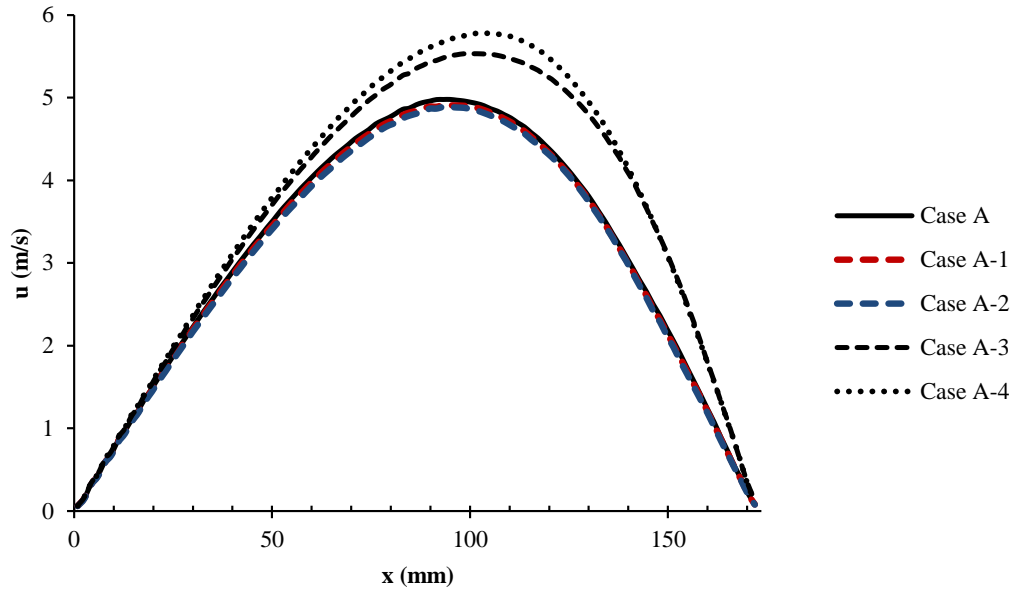
Figure 3.19: Distribution of the axial primary velocity along the enclosure length at y=H/2 at=ωt=π/2 during the 40th acoustic cycle.

The cycle–averaged temperature field for Case A-1, A-2, A-3 and A-4 at t=0.04 s is represented in Figure 3.20. The longitudinal temperature gradients are maximized near the bottom wall and decrease with the increasing distance from the wall for sinusoidal cases. The transverse temperature gradients are relatively higher at x=L/4 and x=3L/4 for Case A-1 and Case A-2. However, the maximum transverse temperature gradient in the enclosure is achieved at x=L/2 for Case A-3 and A-4.

Local Nusselt number along the horizontal walls is defined as:

$$Nu_x = -\frac{H}{T_B(x) - T_T}\frac{dT}{dy}\bigg|_{y=0,H} \qquad (3.2)$$

Where H is the enclosure height, $T_B(x)$ and T_T are the bottom and top wall temperatures, respectively. Evolution of the space-averaged Nusselt number along the horizontal walls with time during the last period for Case A-3, B-3 and C-3 is represented in Figure 3.21. The Nusselt number fluctuations are greater for higher maximum left wall displacement.
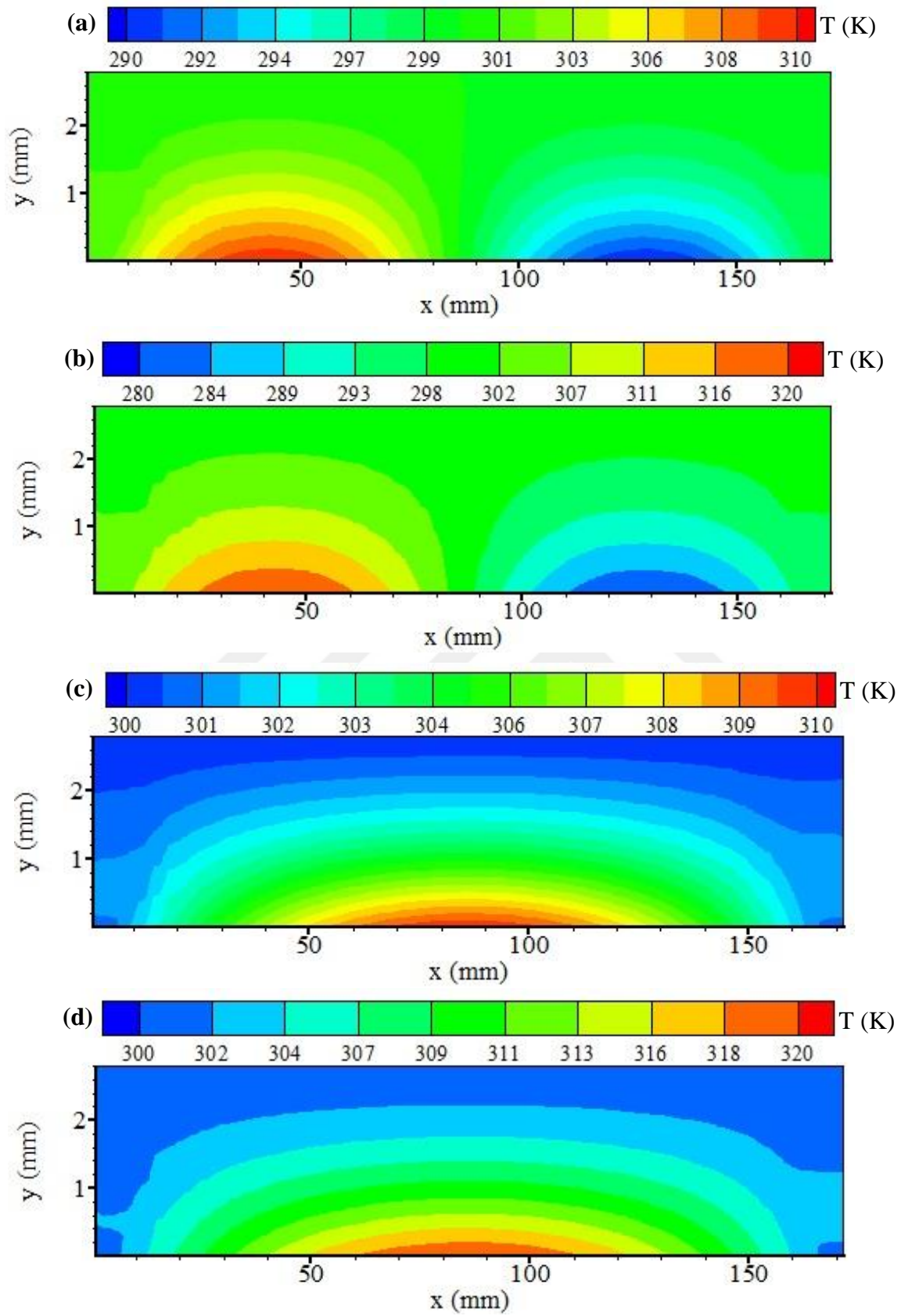
Figure 3.20: Cycle-averaged temperature contours at t=0.04 s for (a) Case A-1, (b) Case A-2, (c) Case A-3 and (d) Case A-4.

(a)

Nu_B

Case A-3
Case B-3
Case C-3

t (s)

(b)

Nu_T

Case A-3
Case B-3
Case C-3

t (s)
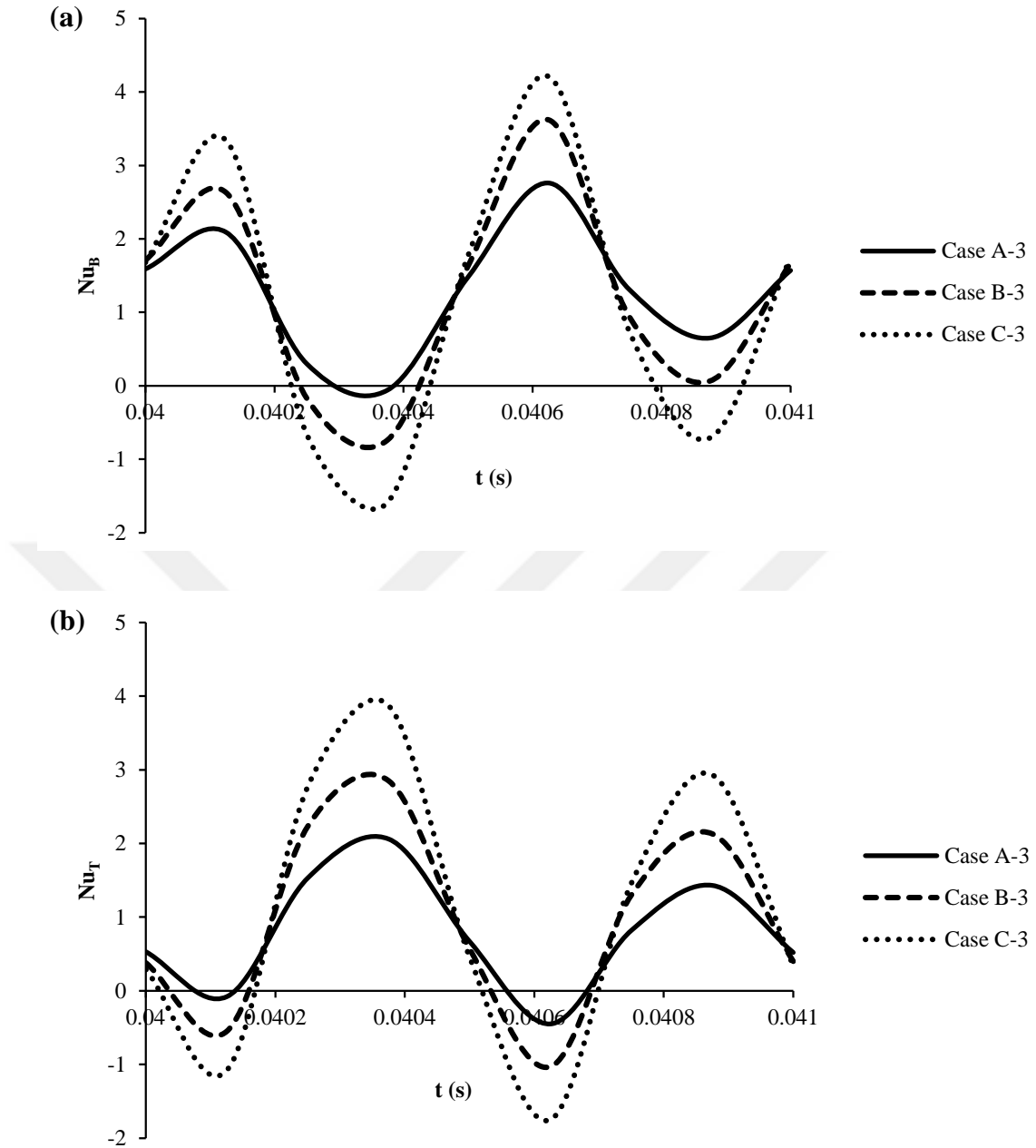
Figure 3.21: Evolution of the spaced-averaged Nusselt number with time at (a) bottom and (b) top walls during the last period for Case A-3, B-3 and C-3.

Figure 3.22 depicts the pressure field in the enclosure at four different instants during the 40th cycle for Case A-3. Harmonic motion of the left wall affects the pressure field in the enclosure. Expansion and compression of air due to the harmonic motion of the left wall leads to fluctuate in the temperature of air. Figure 3.23 represents the temperature field in the enclosure for corresponding instants for Case A-3.
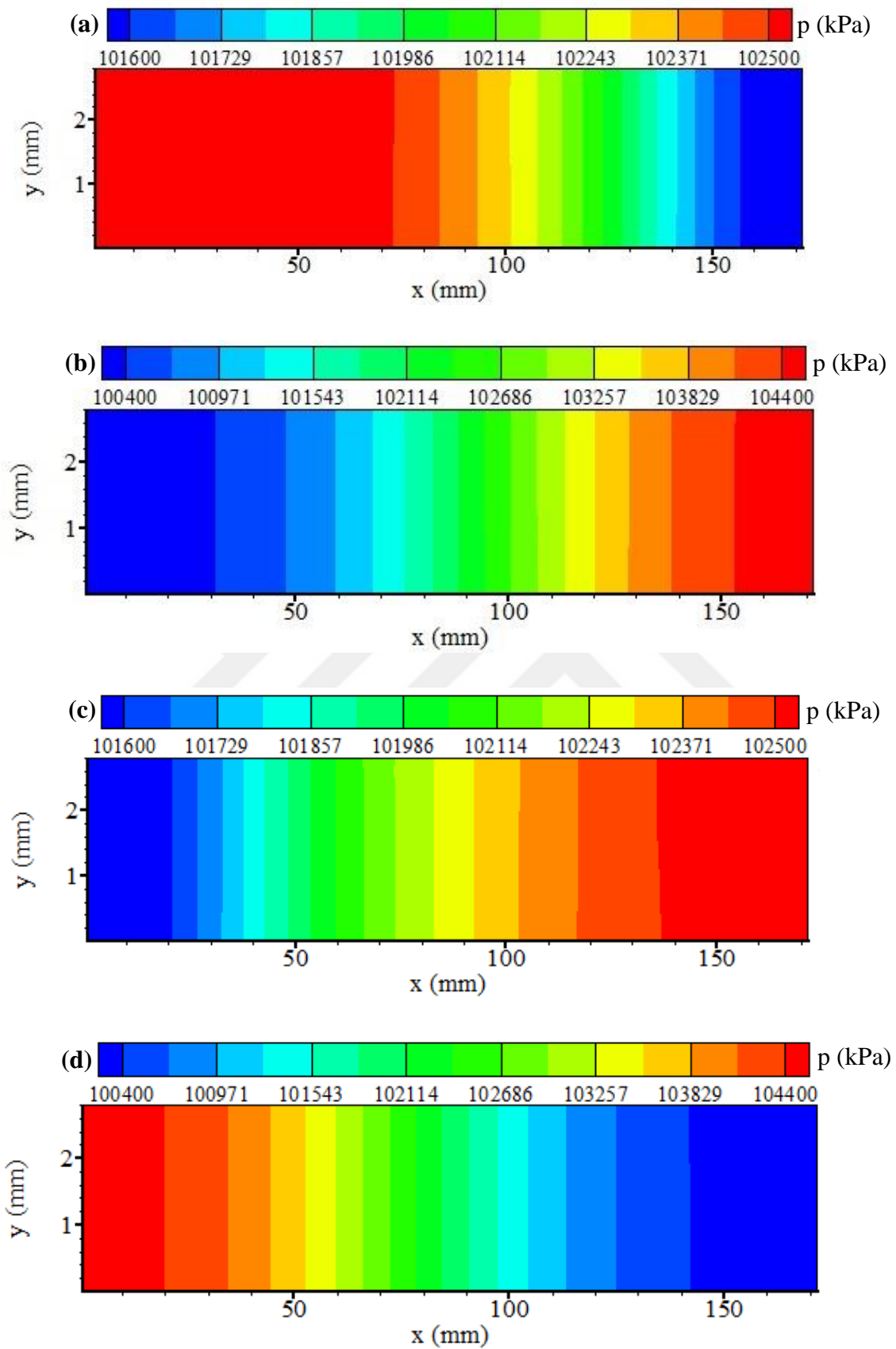
Figure 3.22: Pressure contours in the enclosure during the 40th cycle for Case A-3 at: (a) $\omega t=\pi/2$, (b) $\omega t=\pi$, (c) $\omega t=3\pi/2$ and (d) $\omega t=2\pi$.

46

Figure 3.23: Temperature contours in the enclosure during the 40th cycle for Case A-3 at: (a) ωt=π/2, (b) ωt=π, (c) ωt=3π/2 and (d) ωt=2π.

Table 3.4 lists the magnitude of the Rayleigh streaming velocity, Reynolds number and modified Eckert number for all cases considered. Reynolds number and modified Eckert number are defined as:

$$Re = \frac{1}{2}(\frac{u_{max}}{c})^2(\frac{H}{\delta})^2 \qquad (3.3)$$

$$Ec_m = \frac{u_R^2}{c_p \Delta T} \qquad (3.4)$$

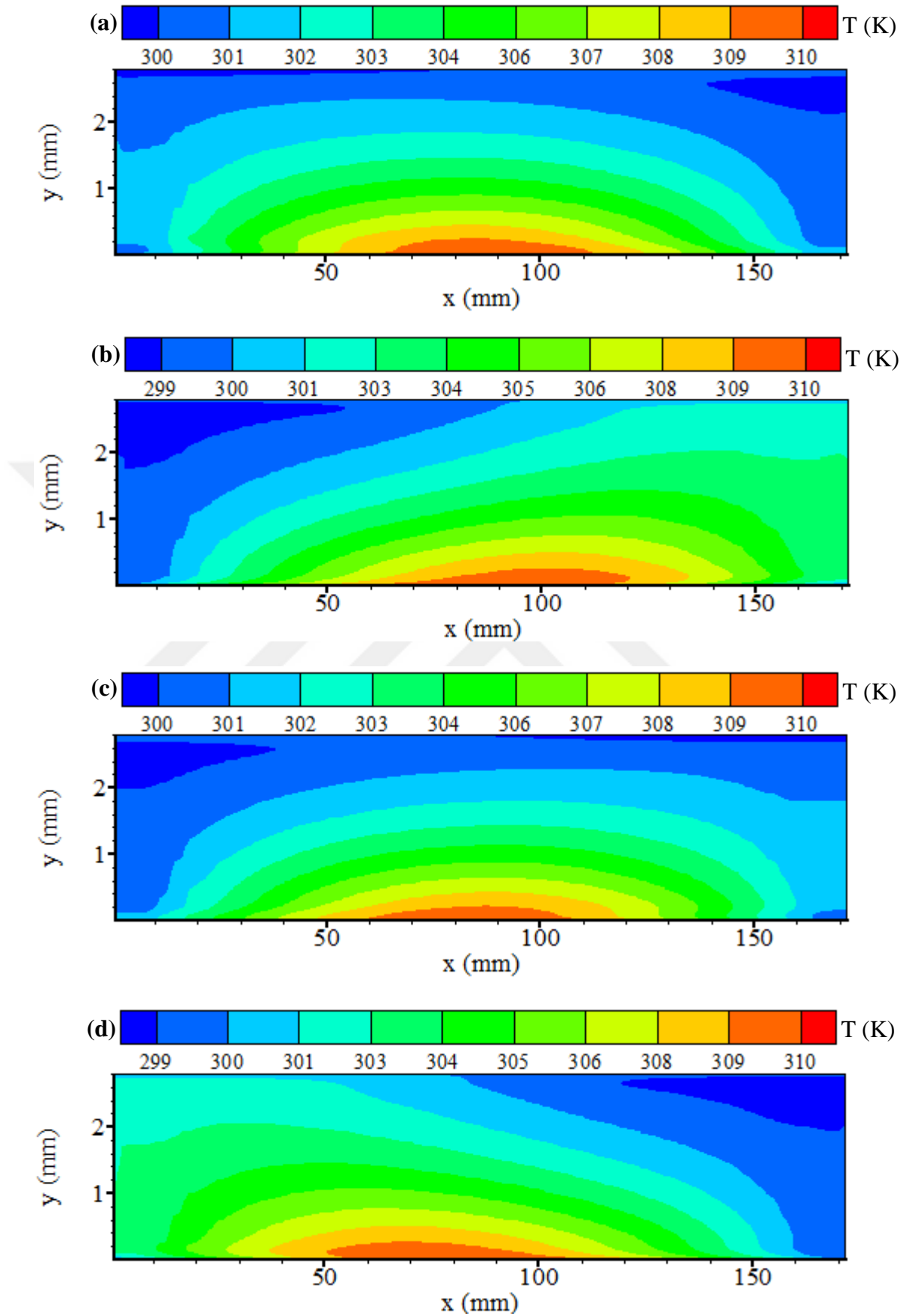Here u_R is the Rayleigh streaming velocity ($u_R = \frac{3u_{max}^2}{16c_0}$) [14], ΔT is the maximum temperature difference between bottom and top walls and c_p indicates the specific heat at constant pressure. In sinusoidal heating cases, for a fixed value of the left wall displacement, magnitude of both Rayleigh streaming velocity and Reynolds number remain same with unheated case.

Table 3.4 : Rayleigh streaming velocity, Reynolds number and modified Eckert number of cases.

Case	Profile	T_{Bmax}(K)	X_{max} (µm)	u_R (m/s)	Re	Ec_m (×10^{-8})
A	isothermal	300		0.01635	0.20	-
A-1	sinusoidal	310		0.01635	0.20	2.66
A-2		320	60	0.01635	0.20	1.33
A-3	half	310		0.0201	0.25	4.02
A-4	sinusoidal	320		0.02213	0.27	2.44
B	isothermal	300		0.0288	0.35	-
B-1	sinusoidal	310		0.0288	0.35	8.26
B-2		320	80	0.0288	0.35	4.13
B-3	half	310		0.03458	0.43	11.9
B-4	sinusoidal	320		0.03722	0.46	6.90
C	isothermal	300		0.04377	0.54	-
C-1	sinusoidal	310		0.04377	0.54	19.1
C-2		320	100	0.04377	0.54	9.55
C-3	half	310		0.0519	0.64	26.8
C-4	sinusoidal	320		0.05622	0.69	15.7

Figure 3.24 represents the variation of the average Nusselt number along the horizontal walls and over the 40th acoustic cycle with modified Eckert number for both horizontal walls. The average Nusselt number for sinusoidal heating cases is computed at the heated portion of the enclosure only. As the Eckert number increases, average Nusselt number decreases at the bottom wall and increases at the top wall for both sinusoidal and half sinusoidal heating cases. The temperature gradient in y-direction at the bottom wall is greater for sinusoidal heating cases. Thus the magnitude of the average Nusselt number is higher in sinusoidal cases relative to the half-sinusoidal cases at constant Eckert number.
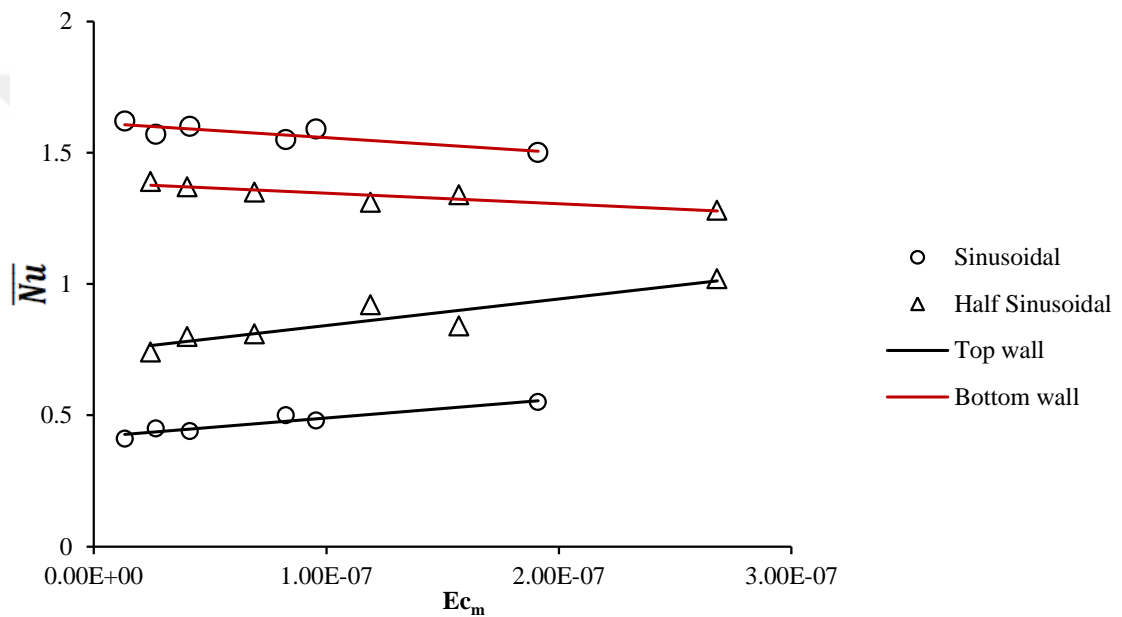
Figure 3.24: Variation of the average Nusselt number with the modified Eckert number at the bottom and top walls.

Figure 3.25 shows the variation of the non-dimensional spaced-averaged steaming velocity gradient (y-component) by modified Eckert number along the bottom and top walls of the enclosure. The streaming velocity gradient is non-dimensionalized by $\frac{H}{u_R}$. The overall y-component of the streaming velocity gradient at the top wall decreases as the Eckert number increases when the bottom wall is subjected to sinusoidal or half-sinusoidal temperature profiles. A positive gradient in the vicinity of the top wall indicates the presence of strong flow towards the bottom wall. Hence reduction in the velocity gradient at the top wall causes to augmentation in Nusselt

number. For the same Eckert number the gradient is higher for sinusoidal cases. This provides lower Nusselt number at the top wall.

Negative sign of the streaming velocity gradient indicates strong flow toward the bottom wall. Magnitude of the Nusselt number decreases as the absolute value of the gradient decreases by increment in the Eckert number. The higher Nusselt numbers are obtained in sinusoidal cases due to the higher absolute streaming velocity gradient compared with half-sinusoidal cases.
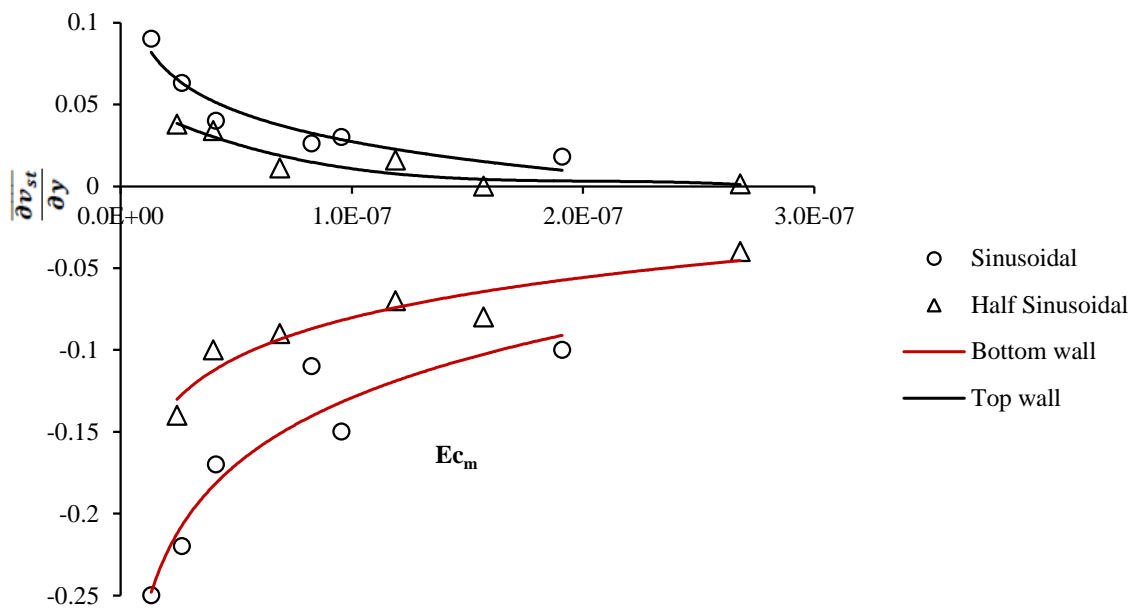
Figure 3.25: Variation of the non-dimensional streaming velocity gradient with the modified Eckert number at the bottom and top walls.

Figure 3.26 presents the variation of the transverse component of the streaming velocity along the enclosure height for half-sinusoidal cases at x=L/2, L/8 and 7L/8. As the velocity amplitude of the vibrating wall and the temperature of the bottom wall increase, air flows towards the heated wall with higher velocity at x=L/2. Direction of the flow is towards the top wall at x=L/8 and x=7L/8.

Distribution of the y-component of the second-order velocity along the vertical lines at x=L/8 and x=7L/8 for sinusoidal cases is shown in Figure 3.27. Streaming velocity is enhanced due to the increase in temperature and left wall displacement amplitude. The direction of the flow is towards the upper section at x=L/8 while it is through the bottom wall at x=7L/8.

50

Figure 3.26: Variation of the y-component of the streaming velocity along the enclosure height for half-sinusoidal cases at (a) x=L/2 (T_{Bmax}=310 and 320 K), (b) x=L/8 and 7L/8 (T_{Bmax}=310 K) and (c) x=L/8 and 7L/8 (T_{Bmax}=320 K).
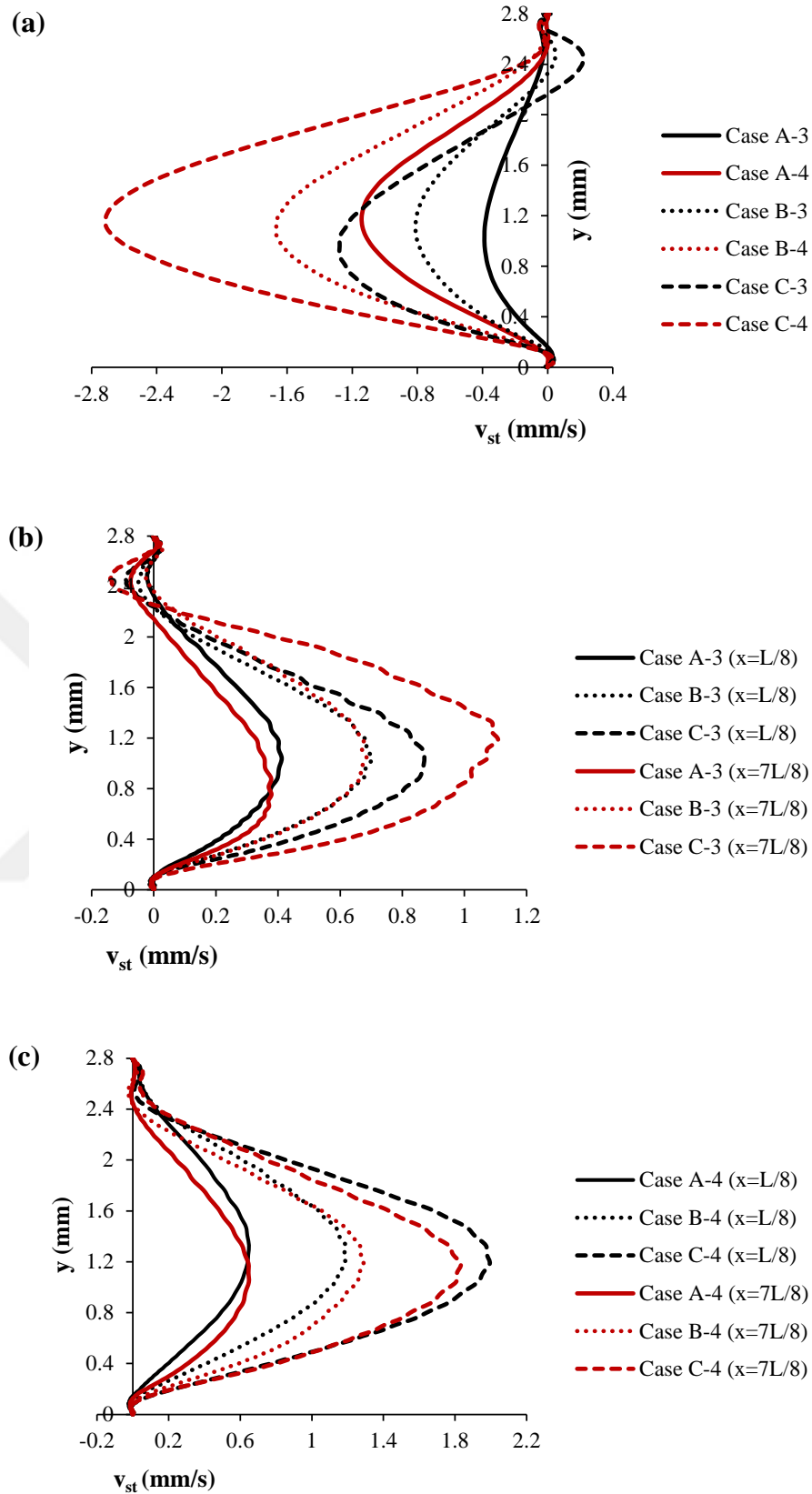
51
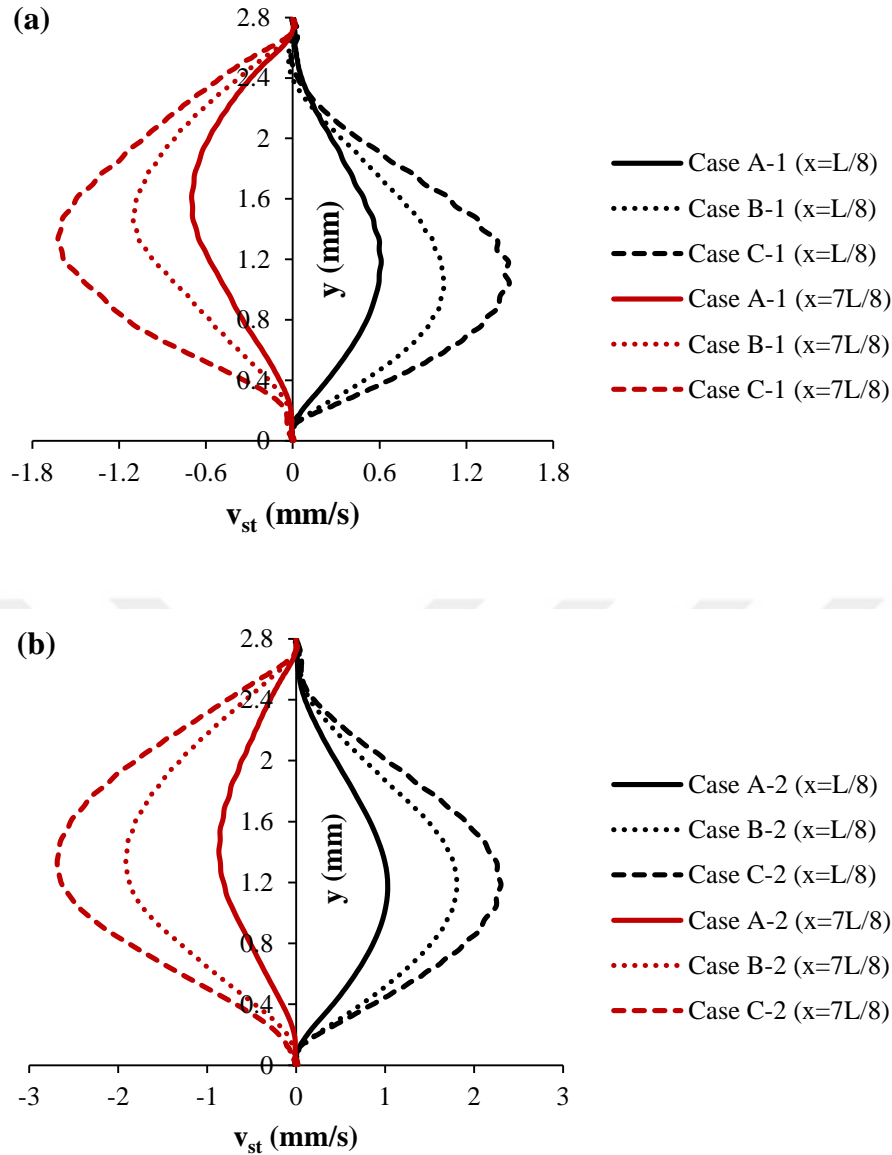
Figure 3.27: Variation of the y-component of the streaming velocity along the enclosure height for sinusoidal cases at (a) x=L/8 and 7L/8 (T_{Bmax}=310 K) and (b) x=L/8 and 7L/8 (T_{Bmax}=320 K).

Figure 3.28 depicts the time-averaged flow field in the enclosure for Case B-1, B-2, C-1 and C-4 at t=0.04 s. As the bottom wall of the enclosure subjected to non-uniform temperature profiles, the symmetry of the streaming structure deforms and streaming velocity increases. The center of the outer vortex in the left portion shifted towards the top wall as the temperature of the bottom wall increases in cases with sinusoidal temperature profiles of bottom wall. However, symmetry respect to the vertical line at x=L/2 can be observed in half-sinusoidal heating cases. Augmentation in the maximum displacement of the vibrating wall also leads to higher velocity in the enclosure.

Figure 3.28: Time-averaged flow field in the enclosure for (a) Case B-1, (b) Case B-2, (c) Case C-1 and (d) Case C-4 at t=0.04 s.

Local heat flux at three different locations of the bottom wall is reported in Table 3.5. In the half-sinusoidal heating cases heat flux decreases as the velocity amplitude of the left wall increases at x=L/8 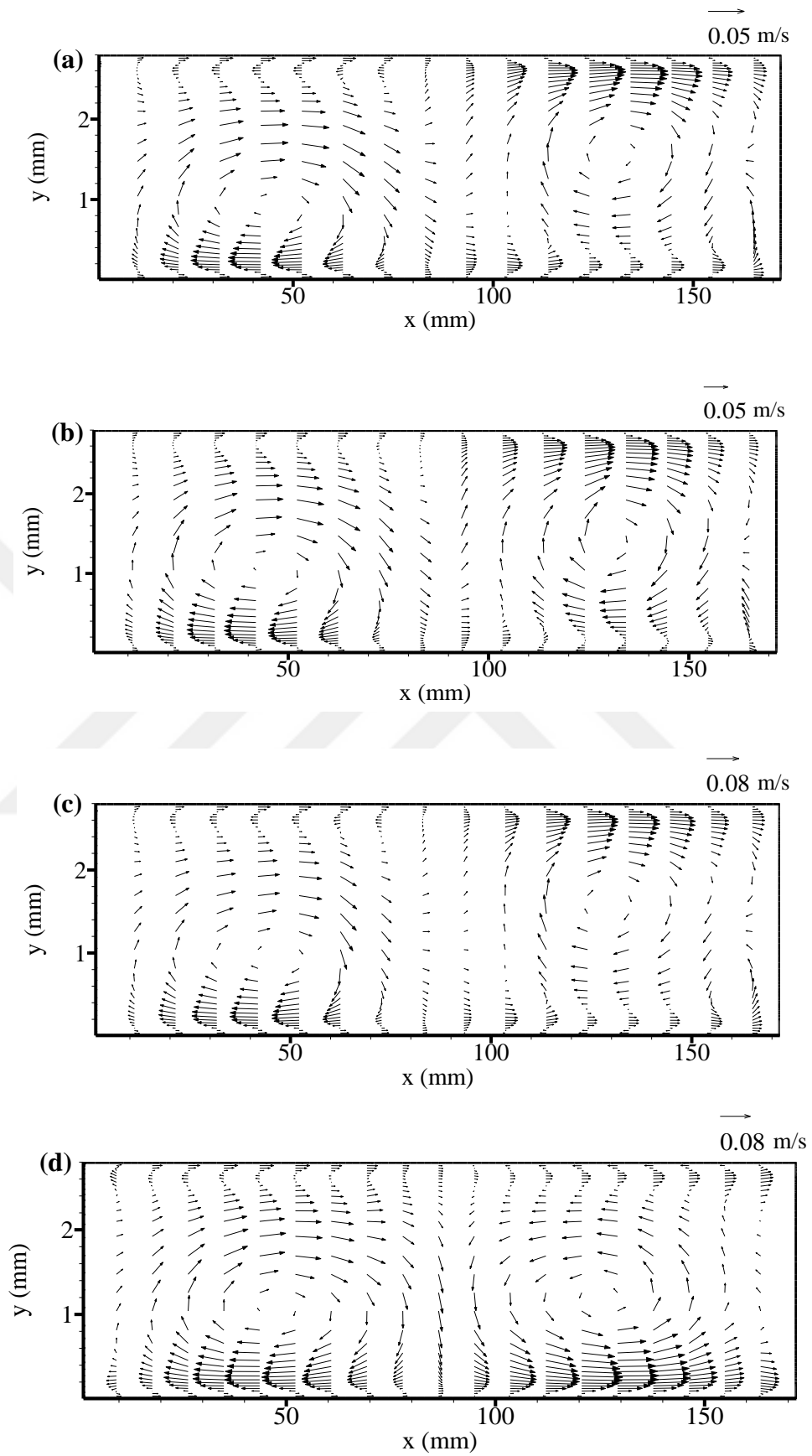and x=7L/8. At these locations bulk streaming flow is towards the isothermal wall as presented in Figure 3.26. Enhancements in heat flux are reported for the same cases at x=L/2 where the air flows through the heated wall. There is no heat transfer at the mid-point of the bottom wall due to the lack of the temperature difference at this location in sinusoidal heating cases. As the displacement of the left wall increases air flows towards the top wall more strongly causes to reduction in heat flux at x=L/8. On the other hand at x=7L/8 the streaming flow is towards the bottom wall and heat flux increases.

Table 3.5 : Local heat fluxes at x=L/8, L/2 and 7L/8 for cases studied.

Case	X_{max} (μm)	q'' (W/m²)		
		x=L/8	x=L/2	x=7L/8
A	60	-	-	-
A-1		96.8	-	120.4
A-2		199.0	-	223.2
A-3		35.6	149.3	36.1
A-4		78.6	300.5	73.6
B	80	-	-	-
B-1		78.8	-	124.9
B-2		180.4	-	231.3
B-3		24.8	150.3	22.9
B-4		60.3	304.7	63.9
C	100	-	-	-
C-1		68.2	-	128.0
C-2		169.3	-	236.3
C-3		15.3	153.4	17.6
C-4		57.2	317.0	52.5

Variation of the total heat transfer per unit depth of the enclosure from the bottom wall for cases with the maximum wall displacement of 60 μm is presented in Figure 3.29. As the time goes on, heat transfer rate decays and sets about the asymptotic value. The heat rate is minimized approximately at t=π/2 and maximized at t=2π during the acoustic cycle. The same behavior can be observed in cases with the maximum wall displacement of 80 and 100 μm which are shown in Figure 3.30 and 3.31, respectively.

Figure 3.29: Temporal variation of the heat rate from the bottom wall for cases with $X_{max} = 60$ μm for (a) all periods and (b) last ten periods.

Figure 3.30: Temporal variation of the heat rate from the bottom wall for cases with X_{max} =80 μm for (a) all periods and (b) last ten periods.
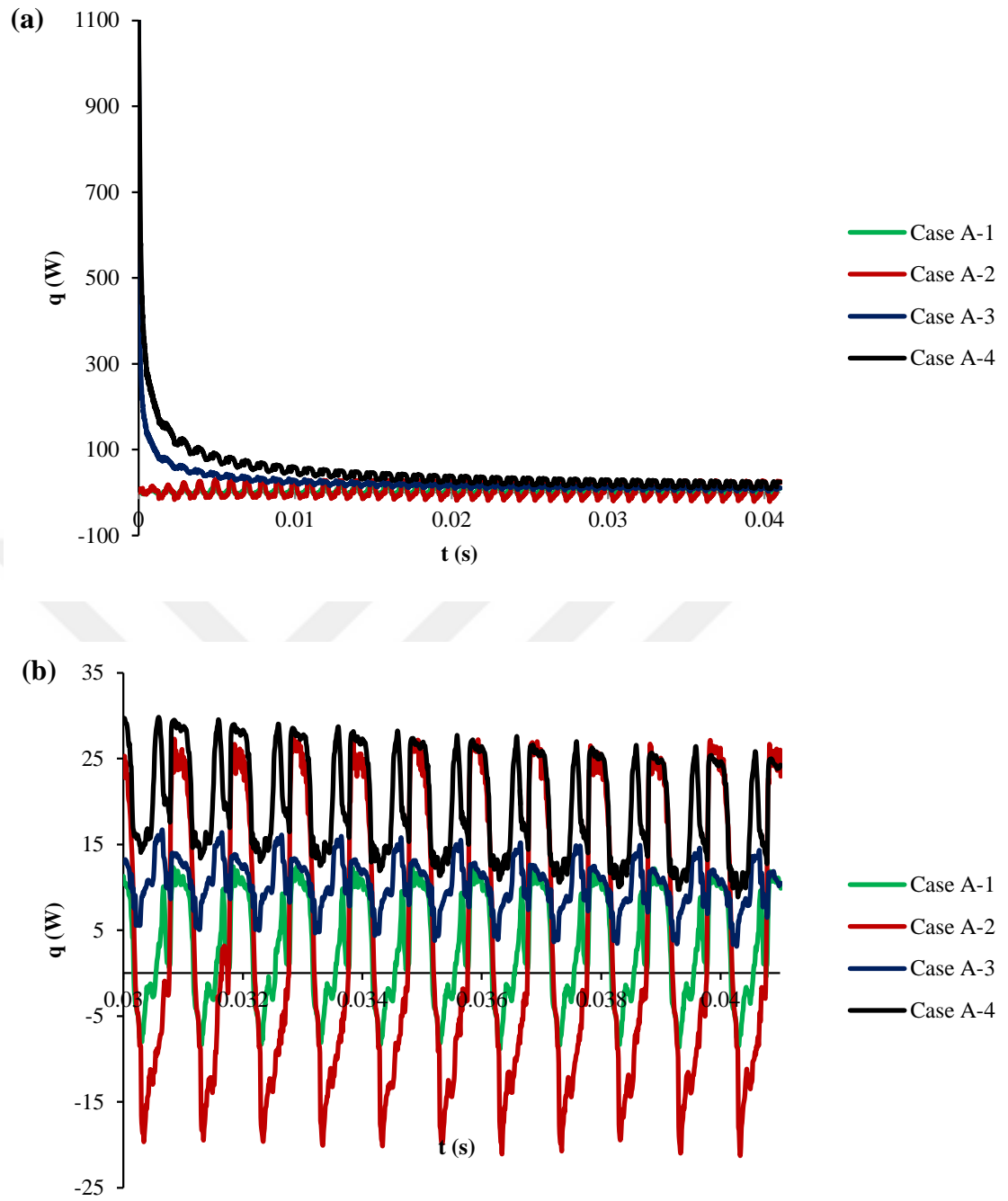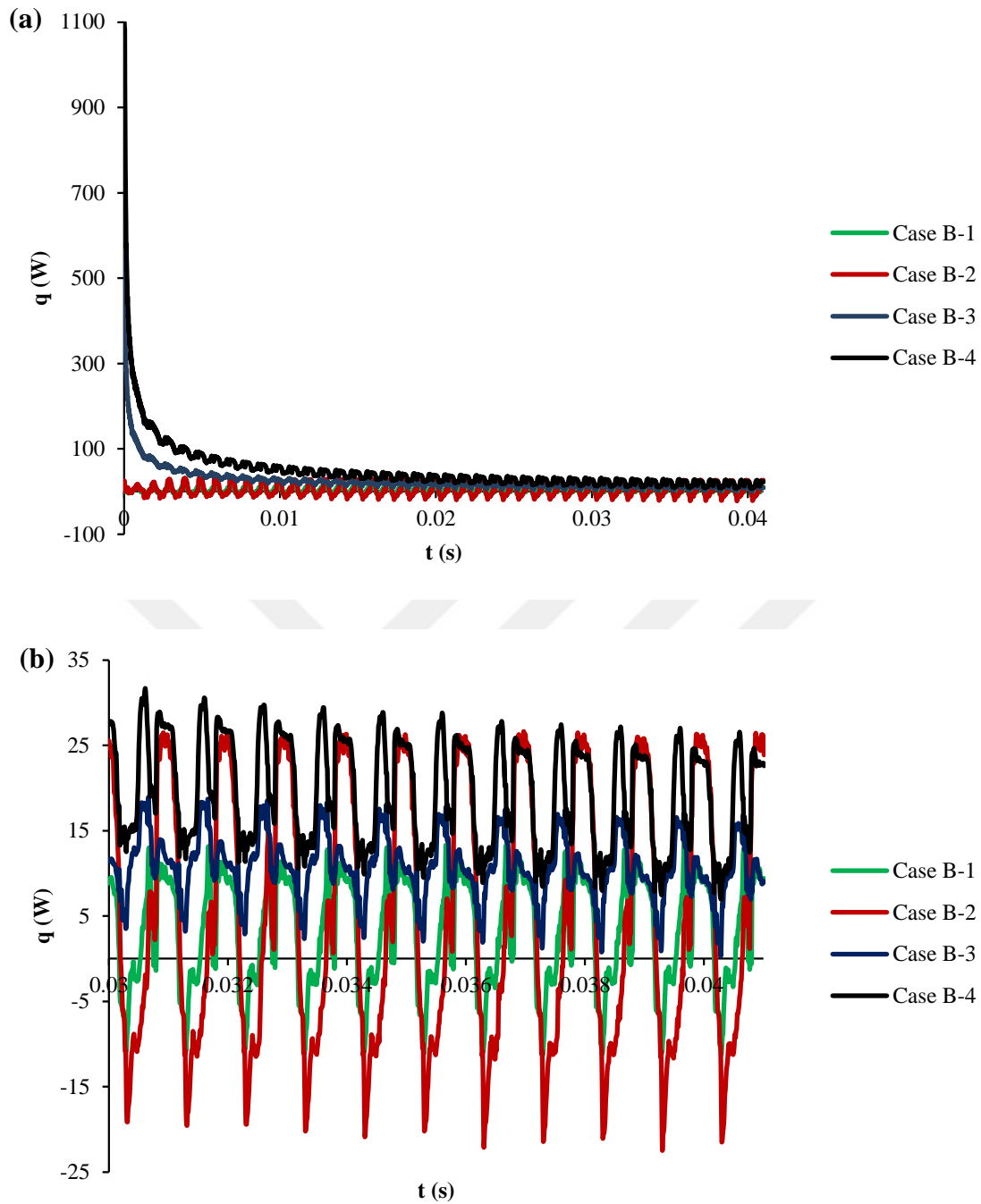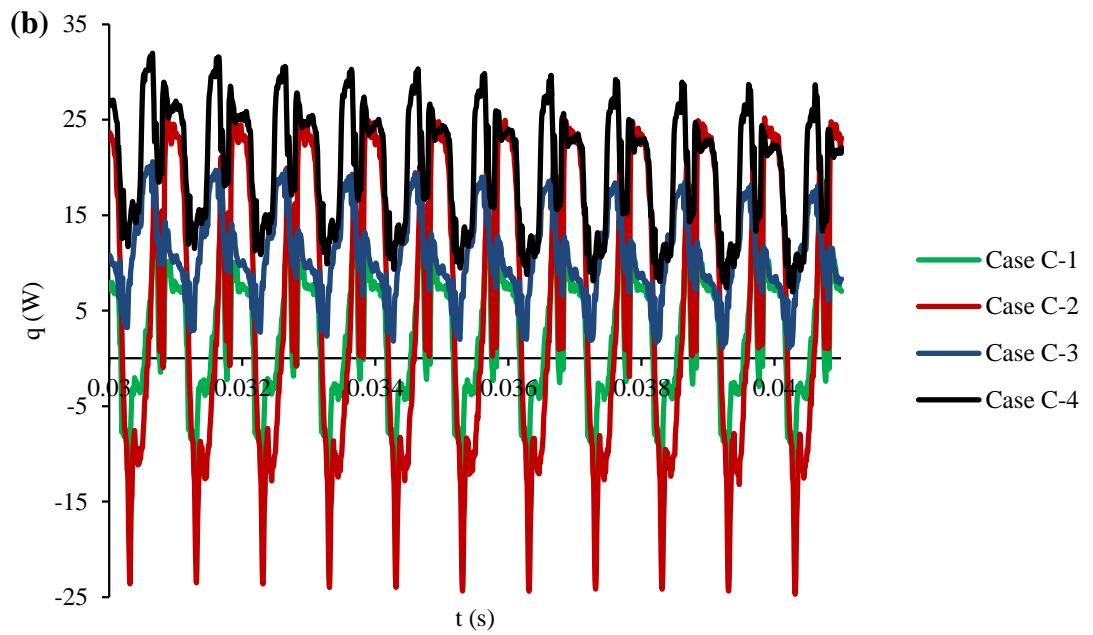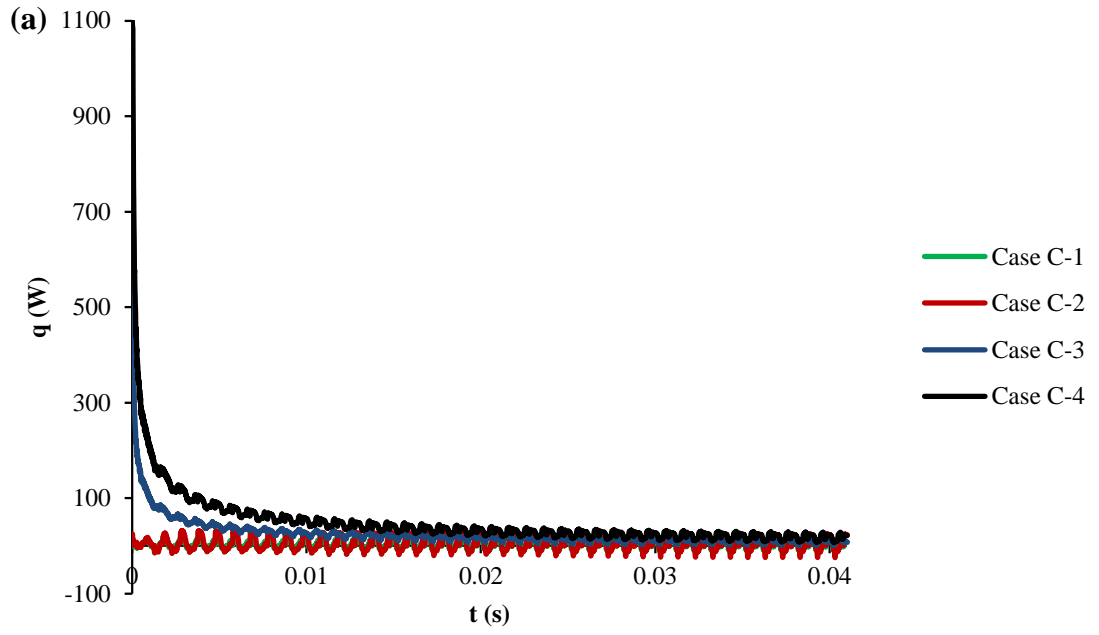
Figure 3.31: Temporal variation of the heat rate from the bottom wall for cases with $X_{max} = 100$ μm for (a) all periods and (b) last ten periods.

4. CONCLUSION

Structure of acoustic streaming and associated heat transfer in a shallow, air-filled, two-dimensional rectangular enclosure, in which the bottom wall is subjected to spatially non-uniform temperature distribution are studied numerically. Formation of acoustic streaming is accomplished by the harmonic vibration of the enclosure left wall. Effects of maximum displacement of the oscillating wall and temperature profiles of the bottom wall on streaming pattern and heat transfer are studied. For unheated cases where the temperature of bottom wall is identical to the top wall temperature, for given enclosure dimensions, increase in the left wall maximum displacement (60, 80 and 100 μm) produces a pressure wave with higher amplitude and enhances the velocity in the enclosure while the streaming structure remains regular. As the temperature of the bottom wall increases, regular streaming shape deforms and complex shape emerges in the enclosure. Structure of these streaming depends strongly on the temperature profile of the bottom wall. Two clock-wise outer vortices almost fill the entire enclosure in sinusoidal heating cases while one counter-clockwise and one clock-wise outer streaming rolls appear in the enclosure in half-sinusoidal cases. Heat transfer rate strongly depends on the streaming structure. In half-sinusoidal cases, the local heat flux from the bottom wall near the vertical walls decreases as the velocity amplitude of the vibrating wall increases due to the flow towards the top wall. However the local heat flux in the vicinity of the stationary vertical wall, where the flow is towards the bottom wall, increases by augmentation in the maximum displacement of the left wall in sinusoidal heating cases. Average Nusselt number along the bottom wall decreases, while an increase can be observed at the top wall as the velocity amplitude of the left wall increases. For a fixed value of the maximum left wall displacement, as the temperature amplitude of the bottom wall is augmented, an increase in the Nusselt number is observed. The gradient of the vertical streaming velocity component is found to be the critical parameter governing the thermal transport in the enclosure.

Analysis of acoustic streaming in presence of non-uniform temperature distribution for wide range of vibration frequency, enclosure aspect ratio can be considered as future work. Also resonators with non-uniform cross-sections can be considered.

REFERENCES

[1] **Halliday, D., Resnick, R., Walker, J.,** (1997). Fundamentals of Physics, 5th Ed., John Wiley & Sons, USA.

[2] **Boluriaan, S., Morris, P.J.,** (2003). Acoustic streaming: from Rayleigh to today, Int. J. Aeroacoustics., 2(3-4), 255-292.

[3] **Lord Rayleigh**, (1884). On the circulation of air observed in Kundt's tubes, Philos. Trans. R. Soc. London, Ser., A175, 1-21.

[4] **Schlichting, H.,** (1932). Berechnung ebener periodischer Grenzschichtströmungen (Calculation on plane periodic boundary layer streaming), Physikalische Zeitschrift, 33(8), 327-335.

[5] **Westervelt, P.J.,** (1953). The theory of steady rotational flow generated by a sound field, J. Acoust. Soc. Am., 25, 60–67.

[6] **Andres, J.M., Ingard, U.,** (1953). Acoustic streaming at low Reynolds numbers, J. Acoust. Soc. Am., 25, 932–938.

[7] **Andres, J.M., Ingard, U.,** (1953). Acoustic streaming at high Reynolds numbers, J. Acoust. Soc. Am., 25, 928–932.

[8] **Kurzweg, U.H.,** (1985). Enhanced heat conduction in oscillating viscous flows within parallel-plate channels, J. Fluid Mech., 156, 291–300.

[9] **Qi, Q.,** (1993). The effect of compressibility on acoustic streaming near a rigid boundary for a plane traveling wave, J. Acoust. Soc. Am., 94, 1090–1098.

[10] **Qi, Q., Johnson, R.E., Harris, J.G.,** (1995). Boundary layer attenuation and acoustic streaming accompanying plane-wave propagation in a tube, J. Acoust. Soc. Am., 97(3), 1499–1509.

[11] **Vainshtein, P., Fichman, M., Gutfinger, C.,** (1995). Acoustic enhancement of heat transfer between two parallel plates, Int. J. Heat Mass Transfer, 38(10), 1893–1899.

[12] **Guo, Z., Sung, H. J,** (1997). Analysis of the Nusselt number in pulsating pipe flow, Int. J. Heat Mass Transfer, Vol. 40, No. 10, 2468-2489.

[13] **Moschandreou, T., Zamir, M.,** (1997). Heat transfer in a tube with pulsating flow and constant heat flux, Int. J. Heat Mass Transfer, 40, 2461-2466.

[14] **Hamilton, M.F., Ilinskii, Y.A., Zabolotskaya, E.A.,** (2003). Acoustic streaming generated by standing waves in two-dimensional channels of arbitrary width, J. Acoust. Soc. Am., 113(1) 153–160.

[15] **Hamilton, M.F., Ilinskii, Y.A., Zabolotskaya, E.A.,** (2003). Thermal effects on acoustic streaming in standing waves, J. Acoust. Soc. Am., 114(6) 3092–3101.

[16] **Kawahashi, M., Arakawa, M.,** (2003). Nonlinear phenomena induced by finite-amplitude oscillation of air column in closed duct, JSME Int. J., 39, 280–286, 1996.

[17] **Frampton, K.D., Martin, S.E., Minor, K.,** (2003). The scaling of acoustic streaming for application in micro-fluidic devices, App. Acoust., 64, 681-692.

[18] **Frampton, K.D., Minor, K., Martin, S.E.,** (2004). Acoustic streaming in micro-scale cylindrical channels, App. Acoust., 65, 1121-1129.

[19] **Aktas, M.K., Farouk, B.,** (2004). Numerical simulation of acoustic streaming generated by finite-amplitude resonant oscillation in an enclosure, J. Acoust. Soc. Am.,116(5), 2822–2831.

[20] **Carlsson, F., Sen, M., Löfdahl, L.,** (2004). Steady streaming due to vibrating walls, Phys. Fluids, 16 (5), 1822–1825.

[21] **Ramos, E., Storey, B.D., Sierra, F., Zuniga, R., Avramenko, A.,** (2004). Temperature distribution in an oscillatory flow with a sinusoidal wall temperature, Int. J. Heat Mass Transfer, 47 (22) 4929–4938.

[22] **Aktas, M. K., Ozgumus, T.,** (2010). The effects of acoustic streaming on thermal convection in an enclosure with differentially heated horizontal walls, Int. J. Heat Mass Transfer, 53, 5289–5297.

[23] **Daru, V., Baltean-Carles, D., Weisman, C., Debesse, P., Gandikota, G.,** (2013). Two-dimensional numerical simulations of nonlinear acoustic streaming in standing wave, Wave Motion, 50, 955-963.

[24] **Cervenka, M., Bednarık, M.,** (2016). Variety of acoustic streaming in 2D resonant channels, Wave Motion, 66, 21-30.

[25] **Ro, P.I., Loh, B.G.,** (2001). Feasibility of using ultrasonic flexural waves as a cooling mechanism, IEEE Trans. Indust. Electron, 48(1), 143–150.

[26] **Alexeev, A., Goldshtein, A.,Gulfinger, C.,** (2002). Heat interaction in a resonance tube, Phys. Fluids, 14 (5), 1812-1815.

[27] **Jun, Z., Danling, Z., Wang, W., Hong, G.,** (2004). An experimental study of heat transfer enhancement with a pulsating flow, Heat Transfer Asian Research, 33(5), 279-286.

[28] **Thompson, M.W., Atchley, A.A.,** (2005). Simultaneous measurement of acoustic and streaming velocities in a standing wave using laser Doppler anemometry, J. Acoust. Soc. Am.117, 1828–1838.

[29] **Thompson, M.W., Atchley, A.A., Maccarone, M.J.,** (2005). Influences of a temperature gradient and fluid inertia on acoustic streaming in a standing wave, J. Acoust. Soc. Am., 117, 1839–1849.

[30] **Hyun, S., Lee., D.R., Loh, B.G.,** (2005). Investigation of convective heat transfer augmentation using acoustic streaming generated by ultrasonic vibrations, J. Heat Mass Transfer, 48, 703-718.

[31] **Wan, Q., Wu, T., Chastain, J., Roberts, W.L., Kuznetsov, A.V., Ro, P.I.,** (2005). Forced convective cooling via acoustic streaming in a narrow channel established by a vibrating piezoelectric bimorph, Flow Turbul. Combust, 74, 195-206.

[32] **Moreau, S., Bailliet, H., Valiere, J. C.,** (2008). Measurements of inner and outer streaming vortices in a standing waveguide using laser doppler velocimetry, J. Acoust. Soc. Am., 123 (2).

[33] **Nabavi, M., Siddiqui, K., Dargahi, J.,** (2009). Analysis of regular and irregular acoustic streaming patterns in a rectangular enclosure, Wave Motion, 46, 312-322.

[34] **Nabavi, M., Siddiqui, K., Dargahi, J.,** (2008). Influence of differentially heated horizontal walls on the streaming shape and velocity in a standing wave resonator, Int. Comm. Heat Mass Transfer 35 (9) 1061–1064.

[35] **Nabavi, M., Siddiqui, K., Dargahi, J.,** (2008). Effects of transverse temperature gradient on acoustic and streaming velocity fields in a resonant cavity, Appl. Phys. Lett. 93 (5) 051902.

[36] **Reyt, I., Daru, V., Baillient, H., Moreau, S., Valiere, J. C.,** (2013). Fast acoustic streaming in standing waves: Generation of an additional outer streaming cell, J. Acoust. Soc. Am., 134(3).

[37] **Tajik, B., Abbasi, A., Saffar-Avval, M., Abdullah, A., Mohammad-Abadi, H.,** (2013). Heat transfer enhancement by acoustic streaming in a closed cylindrical enclosure filled with water, Int. J. Heat Mass Transfer, 60, 230-235.

[38] **Merkin, J.H., Pop, I.,** (2000). Free convection near a stagnation point in a porous medium resulting from an oscillatory wall temperature, Int. J. Heat Mass Transfer 43, 611–621.

[39] **Saeid, N.H.,** (2005). Natural convection in porous cavity with sinusoidal bottom wall temperature variation, Int. Comm. Heat Mass Transfer 32, 454–463.

[40] **Bilgen, E., Yedder, R.B.,** (2007). Natural convection in enclosure with heating and cooling by sinusoidal temperature profiles on one side, Int. J. Heat Mass Transfer 50, 139–150.

[41] **Varol, Y., Oztop, H.F., Pop, I.,** (2008). Numerical analysis of natural convection for a porous rectangular enclosure with sinusoidally varying temperature profile on the bottom wall, Int. Comm. Heat Mass Transfer 35, 56–64.

[42] **Wang, Q.W., Wang, G., Zeng, M., Ozoe, H.,** (2008). Uni-directional heat flux through the horizontal fluid layer with sinusoidal wall temperature at the top or bottom boundaries, Int. J. Heat Mass Transfer 51, 1675–1682.

[43] **Incopera, F.P., Dewitt, P.D., Bergman, L.T., Lavine, S.A.,** (2007). Fundamentals of Heat and Mass Transfer, 6th Ed., John Wiley & Sons, New Jersey.

[44] **Hoffmann, K.A., Chiang, S.T.,** (2000). Computational fluid dynamics Volume I, 4th Ed., USA.

[45] **Boris, J.P., Book, D.L.,** (1976). Solution of the continuity equation by the method of flux corrected transport, Journal of computational physics, 16, pp. 85-129.

[46] **Oran, E.S., Boris, J.P.,** (2001). Numerical Simulation of Reactive Flow, 2nd Ed., Cambridge University Pres, Cambridge.

[47] **Boris, J.P., Landsberg, A.M., Oran, E.S., Gardner, J.H.,** (1993). LCPFCT- A flux-corrected transport algorithm for solving generalized continuity equations, Naval Research Laboratory, Washington, DC NRL/MR/6410-93-7192.

[48] **Poinsot, T.J., Lele, S.K.,** (2000). Boundary conditions for direct simulations of compressible viscous flows. Journal of Computational Physics, 101:104-129, 1992.

RESUME

Personal Information

Surname, Name	: RAHEIMPOUR ANGENEH, Saeid
Nationality	: IRAN
Birth date and Place	: 08.12.1983, IRAN
Marital Status	: Single
Phone	: +90 (507) 666 66 59
E-mail	: raheimpoursaeid@gmail.com

Education

Bachelor of Science **:** 2014, Hacettepe University, Department of Nuclear Energy Engineering.

Master of Science **:** 2017, TOBB University of Economics and Technology, Department of Mechanical Engineering.

Academic Work Experience

2014-2017, TOBB University of Economics and Technology, Department of Mechanical Engineering, Scholarship Student.

Foreign Languages

English, Turkish, Persian

Publications

1. Saeid R. ANGENEH, Murat K. AKTAS, Effect of a vibrating side wall on convective heat transfer in an enclosure with varying bottom wall temperature

distribution, American Physical Society March Meeting 2016, Baltimore, USA, March 14-18,2016.

2. Saeid R. ANGENEH, Murat K. AKTAS, Numerical investigation of vibration-induced thermal convection in an enclosure with spatially non-uniform temperature profile of bottom wall, International Conference On Energy And Thermal Engineering: ISTANBUL 2017, İstanbul, Turkey, April 25-28, 2017.